This is a preprint, the final version is subject to change, of the American Mineralogist (MSA)
Cite as Authors (Year) Title. American Mineralogist, in press.
DOI: https://doi.org/10.2138/am-2018-6339

Revision 2

Experimental investigation of F and Cl partitioning between apatite and Fe-rich basaltic melt at 0 GPa and 950–1050 °C: Evidence for steric controls on apatite-melt exchange equilibria in OH-poor apatite

Francis M. McCubbin[1] and Gokce Ustunisik[2,3]

[1]NASA Johnson Space Center, mailcode XI2, 2101 NASA Parkway, Houston, TX 77058

[2]Department of Geology and Geological Engineering, South Dakota School of Mines and Technology, Rapid City, SD, 57701

[3]Department of Earth and Planetary Sciences, American Museum of Natural History, New York, NY, 10024

Abstract

Apatite-melt partitioning experiments were conducted in a Deltech vertical-quench 1-bar furnace at 0 GPa and 950–1050 °C using an Fe-rich basaltic starting composition. Each experiment had a unique F:Cl ratio to assess the partitioning of F and Cl between apatite and melt, and the oxygen fugacity of all experiments were between IW and IW-1. Apatite-melt partitioning of F and Cl along the F-Cl binary join is investigated in particular to assess the effect of non-ideal mixing of apatite X-site components. The quenched melt and apatite from each experiment were analyzed by electron probe microanalysis. Several of our experiments exhibited evidence of silicate liquid immiscibility (SLI), so we also evaluated the effect of SLI on the partitioning of F and Cl between apatite and melt in those experiments. The F-Cl exchange equilibria between apatite and melt were variable with $K_{d_{Cl-F}}^{Ap-Melt}$ values in the range of 0.08–0.21 across the F-Cl join. The $K_{d_{Cl-F}}^{Ap-Melt}$ values decreased with decreasing F in apatite and melt. Notably, we did not observe evidence that SLI has a first-order effect on the behavior of F and Cl partitioning between apatite

This is a preprint, the final version is subject to change, of the American Mineralogist (MSA)
Cite as Authors (Year) Title. American Mineralogist, in press.
DOI: https://doi.org/10.2138/am-2018-6339

and melt. The observed drop in $K_{d_{Cl-F}}^{Ap-Melt}$ values with decreasing F abundance in melt and apatite indicate that F becomes more compatible in apatite than Cl as there is less F in the system under nominally anhydrous conditions. This behavior can be explained by the presence of an off-mirror F site in F-Cl apatite that only F can occupy, and this F site is required to stabilize the apatite structure in OH-poor systems. These results demonstrate a link between atomic arrangements of apatite X-site components, the thermodynamic mixing properties of apatite X-site components, and the values of apatite-melt exchange equilibria for apatite X-site components. These results also indicate that Cl-rich apatites (i.e., Cl > 0.1 structural formula units (sfu) of apatite X-site) with compositions near the F-Cl binary join (i.e., <0.12 sfu from the F-Cl binary join), even if formed from H_2O-bearing natural systems, should not be used for apatite-based melt-hygrometry.

Introduction

Apatite [$Ca_5(PO_4)_3(F,Cl,OH)$] is present in a wide range of rock types on the Earth (Harlov 2015; Harrison and Watson 1984; Patiño Douce et al. 2011; Piccoli and Candela 2002; Shemesh 1990), and it is also the primary mineralogical host of P in the silicate portion of the planet (Hughes and Rakovan 2002). Along with the nominally volatile-free phosphate mineral merrillite [$Ca_{18}Na_2Mg_2(PO_4)_{14}$], apatite constitutes one of the primary hosts of P in extraterrestrial rocks (McCubbin and Jones 2015). The ubiquity of apatite in planetary materials, coupled with the presence of volatiles (i.e., F, Cl, and OH) in its crystal structure (X-site), has motivated numerous studies to estimate the H_2O abundances of magmas and magmatic source regions in a variety of planetary systems from apatite (Boyce et al. 2010; Filiberto et al. 2016; Gross et al. 2013; McCubbin et al. 2010a, 2012, 2015a, 2016; Patiño Douce and Roden 2006; Patiño Douce et al. 2011; Piccoli and Candela 1994; Tartèse et al. 2013; 2014), a practice referred to as apatite-based melt hygrometry (e.g., Boyce et al. 2014; McCubbin et al. 2015b). However, in order to use the volatile contents of apatite to accurately determine the abundances of volatiles in coexisting silicate melt or fluids, thermodynamic models for the apatite solid solution and for the apatite components in multi-component silicate melts and fluids are required. Although some thermodynamic models for apatite-bearing systems have been developed (i.e., Candela 1986; Hovis and Harlov 2010; Hovis et al. 2014a, 2014b; Li and Hermann 2017; Tacker and Stormer 1989, 1993; Zhu and Sverjensky 1991), they are incomplete and cannot be broadly applied to the full range of geologic conditions under which apatite has formed. Consequently, studies conducting apatite-based melt hygrometry have relied heavily on the results of individual

This is a preprint, the final version is subject to change, of the American Mineralogist (MSA)
Cite as Authors (Year) Title. American Mineralogist, in press.
DOI: https://doi.org/10.2138/am-2018-6339

experimental studies into apatite-melt and/or apatite-fluid partitioning behavior of F, Cl, and OH, which have limited applicability to natural systems.

Numerous modeling and experimental studies have reported apatite-melt or apatite-fluid partitioning relationships for F, Cl, and OH (i.e., Boyce et al. 2014; Brenan 1993; Doherty et al. 2014; Korzhinskiy 1981; Li and Hermann 2015, 2017; Mathez and Webster 2005; McCubbin et al. 2015b; Riker et al. 2018; Webster and Piccoli 2015; Webster et al. 2009, 2017; Zhu and Sverjensky 1991). Although these studies have noted that fluoride is preferred in apatite over chloride, and chloride is preferred in apatite over hydroxyl, this systematic behavior in anion preference in apatite does not translate to constant apatite-melt or apatite-fluid partition coefficients for F, Cl, and OH because the combined abundances of F, Cl, and OH in apatite are fixed by stoichiometry, and the combined abundances of F, Cl, and OH in melt or fluid at apatite saturation are far less constrained (Boyce et al. 2014; McCubbin et al. 2015b). Consequently, a subset of recent studies on apatite-melt partitioning of F, Cl, and OH have described the partitioning of volatiles between apatite and melt as exchange equilibria involving each of the three anion pairs in apatite (i.e., F-Cl, F-OH, Cl-OH; Boyce et al. 2014; Li and Hermann 2015, 2017; McCubbin et al. 2015b; Riker et al. 2018; Webster et al. 2017), similar to the treatment of Fe-Mg partitioning between olivine and silicate melt (Filiberto and Dasgupta 2011; Roeder and Emslie 1970; Toplis 2005). This formalism normalizes the effects of large variations in melt F, Cl, and OH abundances on apatite-melt partition coefficients, which allows for a clearer evaluation of the partitioning behavior. Although the F-Cl, Cl-OH, and F-OH apatite-melt exchange coefficients exhibit substantially less variability than individual apatite-melt partition coefficients (Li and Hermann 2015, 2017; McCubbin et al. 2015b; Webster et al. 2017), non-Nernstian partitioning behavior is observed in some experiments and has been hypothesized to

This is a preprint, the final version is subject to change, of the American Mineralogist (MSA)
Cite as Authors (Year) Title. American Mineralogist, in press.
DOI: https://doi.org/10.2138/am-2018-6339

result from non-ideal mixing of F, Cl, and OH in apatite (Li and Hermann 2017; McCubbin et al. 2015b).

In the present study, we seek to gain a better understanding of apatite-melt partitioning relationships in portions of apatite compositional space where X-site components undergo non-ideal mixing. To accomplish this goal, we conducted apatite-melt partitioning experiments in vacuum-evacuated, sealed silica-glass tubes at ~ 0 GPa and 950–1050 °C on a synthetic martian basalt composition equivalent to the basaltic shergottite Queen Alexandria Range (QUE) 94201, which is the same starting composition used by McCubbin et al. (2015b). These experiments were conducted dry and at low pressure to assess the effects of temperature and apatite composition on the partitioning behavior of F and Cl between apatite and basaltic melt along the F-Cl apatite binary join. We focus on this join in particular for two reasons: 1) solution calorimetry data of apatite along the F-Cl join exhibit excess enthalpies of mixing as high as 8.3 kJ/mol (Hovis and Harlov 2010), and 2) apatites with compositions along or near the F-Cl join occur in numerous samples from Earth and beyond (Hovis and Harlov 2010; McCubbin and Jones 2015), so this study will have direct relevance to the interpretation of apatite compositions in those samples.

Experimental and Analytical Methods

Starting materials

One of the primary goals of the present study is to assess apatite-melt partitioning as a function of apatite X-site occupancy. This goal requires that the starting materials have flexibility in their F:Cl ratio. An additional goal of the present study is to compare our results directly with those of our previous work on apatite-melt partitioning (McCubbin et al. 2015b). To accomplish both of these goals, two powdered mixtures that were used in McCubbin et al. (2015b) were also

This is a preprint, the final version is subject to change, of the American Mineralogist (MSA)
Cite as Authors (Year) Title. American Mineralogist, in press.
DOI: https://doi.org/10.2138/am-2018-6339

used for the present study. One mixture represents an F endmember and the other a Cl endmember, with approximately 1 wt.% of F or Cl, respectively (Table 1). Both starting materials had a single base composition modeled after the Fe-rich basaltic shergottite QUE 94201 (from Kring et al. 2003) with approximately 5 wt.% additional P_2O_5 component to induce early phosphate saturation. The mixtures were generated by accurately weighing silicates, oxides, $Ca_2P_2O_7$, CaF_2, and $MgCl_2$ powders in the proportions needed for obtaining the desired starting compositions. Carbonate starting materials were avoided to prevent unwanted CO-species in the system. The reader is referred to McCubbin et al. (2015b) for additional details concerning the preparation of both starting materials.

Deltech vertical-quench 1-bar furnace experiments

Experiments were conducted in the experimental petrology lab at Lamont-Doherty Earth Observatory of Columbia University. All of the experiments were conducted in Deltech vertical-quench gas-mixing furnaces, although we did not use the gas-mixing function of the furnaces in the present study. For each of our experiments, ~7.5 milligrams of starting material consisting of various ratios of F- and Cl- mixtures (F:Cl ratio of 90:10, 75:25, 50:50, 25:75, 10:90) were loaded into high purity molybdenum metal capsules with tight-fit lids. The capsules were approximately 1 mm wide and 3 mm long, and each capsule was cleaned ultrasonically in acetone to remove any machining residue before use. During the capsule-loading process, the powders were tapped down with a piston in order to pack the powder as densely as possible to minimize pore space. Filled capsules were then weighed and placed into a silica glass tube from Thomas Scientific that we had already sealed at one end. Glass spacers (12.5 mm and 25 mm in length) were placed just above the capsule to minimize the extra volume inside the silica tube and facilitate the process of making a capillary. After evacuating the partially sealed silica tube

This is a preprint, the final version is subject to change, of the American Mineralogist (MSA)
Cite as Authors (Year) Title. American Mineralogist, in press.
DOI: https://doi.org/10.2138/am-2018-6339

for 15 minutes to remove as much air as possible, the tube was heated using a H_2–O_2 torch and stretched to form a small capillary. The torch was used to sever and seal the capillary just above the glass spacers, preserving a vacuum in the silica glass ampoule. The attached capillary was then curved into a hook for eventual suspension in the furnace. The silica tube was suspended across a thin Pt-wire through the hook at the top of the ampoule and placed at the hotspot of the furnace. Temperature was controlled by PID feedback using a $Pt_{70}Rh_{30}$-$Pt_{94}Rh_6$ (type B) thermocouple in the furnace cavity. A $Pt_{90}Rh_{10}$-Pt (type S) thermocouple calibrated against the melting point of Au, Li metasilicate, and diopside was used to monitor the temperature of the sample. The thermocouple was positioned such that its tip was directly adjacent to the capsule. The capsule and thermocouple were gradually lowered into the pre-heated furnace (1150 °C) in order to minimize thermal shock to the system. Horizontal temperature differences at the hot spot were within 1°C of the set point. In the case of identical run temperatures for different starting compositions, multiple charges were hung simultaneously at the corners of horizontal 10–15 mm ceramic bars within the hot spot.

Each experimental charge was held at a melting temperature of 1150 °C for 30 minutes before the temperature was lowered to the crystallization temperature of interest at either 950 °C, 1000 °C, or 1050 °C at a rate of 15 °C/min, where it dwelled for 8 hours. A dwell time of 8 hours was selected in the present study to ensure that a steady-state was reached with respect to F-Cl apatite-melt exchange coefficients. Our previous experiments on apatite-melt partitioning indicate that a steady state is reached by approximately 2 hours of dwell time (McCubbin et al. 2015b). At the end of each experiment, the sample was drop-quenched into a beaker of cold water by passing a current through the Pt-wire supporting the sample. Before each silica glass tube was opened, they were checked to ensure a vacuum was maintained after quench. The silica

This is a preprint, the final version is subject to change, of the American Mineralogist (MSA)
Cite as Authors (Year) Title. American Mineralogist, in press.
DOI: https://doi.org/10.2138/am-2018-6339

tube was opened by lightly crushing the end of the silica tube after the quenched sample was weighed. Samples were encased in epoxy without removing them from the capsule, and the cured epoxy mounts were polished for analysis by electron probe microanalysis (EPMA). All experiments, their run conditions, including starting compositions, capsule material, duration, crystallization temperatures, and phases present, are listed in Table 2.

Although the oxygen fugacity (f_{O2}) was not buffered in our experiments, the Mo^0 capsule materials should affect the f_{O2}. At the end of each experiment, Mo^0 capsule material was in contact with quenched glass, indicating the experiments were at or below the Mo-MoO_2 (MMO) buffer, which is approximately equal to the IW buffer at 0 GPa and 950–1050 °C (O'Neill, 1986; O'Neill and Pownceby 1993). The minimum oxygen fugacities for each experiment cannot be directly determined. However, the experiments are all likely to be above ΔIW-1 given the elevated abundances of FeO in the melt (17.15–26.86 wt.% FeO) and the absence of Fe metal, both as a separate phase or as a measurable component in the Mo metal (as determined by energy dispersive spectroscopy).

Electron probe microanalysis (EPMA)

Apatites and quenched glasses in the experimental run products were analyzed using either a JEOL JXA 8200 electron microprobe in the Institute of Meteoritics at the University of New Mexico or a JEOL 8530 field emission electron microprobe at NASA's Johnson Space Center. An accelerating voltage of 15 kV and a nominal beam current of 20 nA were used during each analysis, following procedures previously established by our group for the analysis of apatite and halogen-bearing glasses (i.e., McCubbin et al. 2010b, 2011, 2015b). At UNM, the elements Si, Ti, Al, Cr, Mg, Fe, Mn, Ca, Na, P, F, and Cl were analyzed in the glasses and Si, Al, Mg, Fe, Mn, Ca, Na, P, F, and Cl in apatite. At JSC the elements Si, Ti, Al, Cr, Mo, Mg, Fe, Mn,

This is a preprint, the final version is subject to change, of the American Mineralogist (MSA)
Cite as Authors (Year) Title. American Mineralogist, in press.
DOI: https://doi.org/10.2138/am-2018-6339

Ca, Na, P, F, and Cl were analyzed in glasses and Si, Al, Mg, Fe, Mn, Ca, Na, P, F, and Cl in apatite. Fluorine was analyzed using a light-element LDE1 detector crystal, and Cl was analyzed using a PET detector crystal. Calcium and P were standardized using the Wilberforce apatite. Fluorine was standardized on SrF_2, and Ap020 (McCubbin et al. 2012) was used as a secondary check for F. Chlorine was standardized with sodalite from Sharp et al. (1989) or on Tugtupite from SPI Supplies, and scapolite from the Smithsonian (NMNH R6600-1) was used as a secondary standard (Jarosewich et al. 1980). Manganese was standardized using Taylor spessartine garnet (Taylor standard block, information from Taylor multi element standard documentation, by C.M. Taylor, C.M. Taylor Company) or rhodonite from SPI supplies. Aluminum was standardized using Taylor pyrope or Sitkin anorthite. Iron was standardized with ilmenite from the Smithsonian (NMNH 133868 and NMNH 96189). Magnesium was standardized using the Taylor olivine and Springwater olivine (NMNH 2566). Sodium was standardized using the Taylor albite and albite from SPI Supplies. Silicon was standardized on Taylor quartz and diopside from SPI Supplies. Chromium was standardized on Taylor chromite and chromite from the Smithsonian (NMNH 117075). Titanium was standardized using Taylor rutile and rutile from SPI Supplies. In order to reduce or eliminate electron beam damage, we used a 10 μm defocused beam for standardization and 1 to 5 μm diameter beam for analysis of apatite grains due to their small size. A 5 μm defocused beam was used for analysis of quenched glass in all samples. Our previous studies on apatite show that standardization at 10 μm is applicable to analyses of apatite with 1 μm beam diameter (McCubbin et al. 2016).

Stormer et al. (1993) documented that F and Cl X-ray count rates change with time during EPMA of apatite as a function of crystallographic orientation. Goldoff et al. (2012) presented a method to minimize changes in count rate for F and Cl. However, the apatites

This is a preprint, the final version is subject to change, of the American Mineralogist (MSA)
Cite as Authors (Year) Title. American Mineralogist, in press.
DOI: https://doi.org/10.2138/am-2018-6339

analyzed in the present study were too small (1–10 μm in the shortest dimension) to apply this technique. Accordingly, we monitored apatite analyses for time-dependent count rates using Probe for EPMA (PFE) software following the procedures of McCubbin et al. (2010b). Fluorine count rates were not always constant during the course of an analysis. Chlorine count rates, on the other hand, were constant for all of our analyses, consistent with the findings of McCubbin et al. (2010b, 2013). For the analyses that exhibited variable F X-ray count variation we used a time-dependent intensity (TDI) correction in the PFE software using the methods described in McCubbin et al. (2010b). Any analyses that displayed highly variable F X-ray count rates (e.g., Figure 2f in McCubbin et al. 2010b) or non-linear and negative changes in F X-ray count rates during the course of an analysis (e.g., Figure 2d in McCubbin et al. 2010b) were rejected. Even with this criterion, some of the apatites contained more than their stoichiometric amount of F + Cl. In these cases, we were able to obtain only a minimum Cl:F ratio by assuming $1 - X_{Cl} = X_F$, after McCubbin et al. (2011). This adjustment in the measured F:Cl ratio is only applicable because we did not observe variability in the Cl X-ray count rates during any of the apatite analyses in the present study.

The quality of each apatite analysis was assessed based on EPMA totals, stoichiometric constraints, and abundances of SiO_2 and Al_2O_3 in apatite. If analytical totals were outside of the range 97.0–102.0 wt.%, the analysis was discarded. The leniency on analytical total deficiency is due to the possibility of vacancies or O^{2-} substitution in the X-site of F-Cl apatite, which cannot be accurately quantified by the EPMA technique. If the stoichiometry of the P or Ca sites deviated by more than ±2% (i.e., 0.06 structural formula units (sfu) or 0.10 sfu on a 13 anion basis for the P- and Ca-sites, respectively), the analysis was discarded. Finally, if SiO_2 or Al_2O_3 abundances were greater than 2 wt.% or 0.5 wt.%, respectively, the analysis was discarded

This is a preprint, the final version is subject to change, of the American Mineralogist (MSA)
Cite as Authors (Year) Title. American Mineralogist, in press.
DOI: https://doi.org/10.2138/am-2018-6339

because it signifies substantial overlap with surrounding quenched glass. However, in some cases we conducted a glass subtraction routine to deconvolve an apatite composition using the techniques outlined in McCubbin et al. (2009, 2013). Nonetheless, glass-subtracted apatite compositions were not used in any sample averages (i.e., Table S1), and the glass-subtracted apatite data were only used where explicitly identified.

We computed a missing component in the X-site of apatite on the basis of stoichiometry if the sum of F and Cl was less than 1 sfu. If both F and Cl are analyzed with sufficient accuracy, this missing component can be attributed to some combination of the anions OH^-, O^{2-}, CO_3^{2-}, S^{2-}, Br^-, and I^- and/or structural vacancies (Pan and Fleet 2002) and/or structural H_2O (Mason et al. 2009). However, we included only Cl and F constituents in our experiments, and we anticipate low amounts of OH contamination based on the low solubility of H-species in silicate melts at low pressure (Burnham 1994; Newcombe et al. 2017). Consequently, we anticipate minimal OH in our magmatic apatite crystallized at 0 GPa. Furthermore, Cl-rich apatites along the F-Cl join commonly exhibit a missing component that can be attributed to O^{2-} and/or structural vacancies (Hovis and Harlov 2010; Jones et al. 2014, 2016; Schettler et al. 2011), so we depict this missing component as X_{other} rather than presume it is OH^-. Importantly, our analytical routine for measuring F and Cl by EPMA is imperfect, and a missing component is not considered to be detected unless it exceeds 0.08 sfu (McCubbin et al. 2010b).

Results

Each experiment resulted in some combination of pyroxene, silica, ilmenite, apatite, plagioclase, hercynitic spinel, and melt. Additionally, five of the experimental run products (Q1b.002, Q1b.003, Q1b.006, Q1b.009, and Q1b.012) have either two distinct melt phases or large variations in melt composition, indicating they either underwent silicate liquid

This is a preprint, the final version is subject to change, of the American Mineralogist (MSA)
Cite as Authors (Year) Title. American Mineralogist, in press.
DOI: https://doi.org/10.2138/am-2018-6339

immiscibility (SLI) or incomplete homogenization during crystallization (Figure 1b, d). The assemblage present in each experimental run product is listed in Table 2.

The primary focus of our study is apatite-melt partitioning of F and Cl, so we focus on the textures and compositions of the apatite and melt phases in each experiment. The apatites are distributed throughout the experimental run products and occur as small, highly acicular, prismatic crystals that ranged in width (short dimension) from about 1 to 10 μm with aspect ratios of about 1:10 to 1:50 (Figure 1). The largest apatites that grew from the silicate melt were approximately 10 μm in the shortest dimension and approximately 100–150 μm in the longest dimension (Figure 1). The average apatite and melt compositions from each experiment are provided in Table S1. In addition, we report the melt compositions from each of the experiments that exhibited large ranges in melt composition in Tables S2–S6, along with any corresponding apatite-melt pairs in Tables S7–S10 to assess local apatite-melt partitioning of F and Cl in the experiments with large variations in melt composition. All of the apatite analyses from the present study are included in Table S11, along with the computed apatite stoichiometry on the basis of 13 anions. Finally, all of the melt analyses from the present study are included in Table S12.

Composition of apatite from experiments

The average compositions of apatite from each experiment, as determined by EPMA, are provided in Table S1, and a compilation of all apatite analyses from the present study are provided in Tables S11. Apatite compositions from each experiment exhibited fairly limited intrasample variation (Table S1), even in experiments that had large variations in melt composition. Nonetheless, we have reported apatite-melt pairs from the experiments that exhibited large ranges in melt composition Table S7–S10. By varying the proportions of F and

This is a preprint, the final version is subject to change, of the American Mineralogist (MSA)
Cite as Authors (Year) Title. American Mineralogist, in press.
DOI: https://doi.org/10.2138/am-2018-6339

Cl in the starting composition, we grew apatites spanning much of the F-Cl join in our series of experiments with Cl abundances in apatite ranging from 0.24 to 5.69 wt.% Cl and F abundances in apatite ranging from 0.28 to 3.63 wt.% F (Table 3). Moreover, all of the apatites with more than 0.52 sfu Cl have a detectable missing component in the apatite X-site (Table 3) that we presume to be an O^{2-} + vacancy substitution given the paucity of H in the system and the observation of OH-poor, X-site-deficient, Cl-rich, F-Cl apatites in natural and synthetic systems (Hovis and Harlov 2010; Jones et al. 2014, 2016; Schettler et al. 2011). Similar to the apatites produced in experiments by McCubbin et al. (2015b), the apatite compositions have elevated abundances of Fe and Mg compared to endmember Ca-apatite with FeO abundances ranging from 1.91 to 5.11 wt.% and MgO abundances ranging from 0.79 to 1.26 wt.%. The apatites also had trace to minor abundances of SiO_2, MnO, and Na_2O, with 0.34 to 1.92 wt.% SiO_2, 0.16 to 0.47 wt.% MnO, and 0.03 to 0.28 wt.% Na_2O. These apatite compositions are similar to those observed in samples from numerous terrestrial worlds across the Solar System, including, Earth, Moon, Mars, Vesta, and ordinary chondrite parent bodies (Harlov et al. 2006; Jones et al. 2014, 2016; Lewis and Jones 2016; McCubbin and Jones 2015; McCubbin et al. 2015a, 2016; Piccoli and Candela 2002; Sarafian et al. 2013).

Composition of quenched melt from experiments

The average compositions of melt from each experiment, as determined by EPMA, are provided in Table S1, and a compilation of all melt analyses from the present study are provided in Tables S12. The EPMA totals for some of the glass analyses, particularly those collected at UNM, were low and variable within individual experimental run products (Table S11), however normalized totals exhibited much less variation except in cases where variation in melt composition was apparent from back-scattered electron images. We suspected that the low totals

This is a preprint, the final version is subject to change, of the American Mineralogist (MSA)
Cite as Authors (Year) Title. American Mineralogist, in press.
DOI: https://doi.org/10.2138/am-2018-6339

were due, in part, to an extra-thick carbon coat, although we could not rule out substantial Mo contamination from the capsules. To further elucidate this issue, we conducted additional analyses of our samples at JSC after re-polishing and re-coating the samples, and we included Mo in the analysis routine. The Mo abundances in our quenched glasses were low and cannot make up for the low totals, which is to be expected based on existing models for Mo solubility in silicate melts (Holzheid et al. 1994). Furthermore, the totals on the re-coated samples were much higher than the data collected at UNM (Table S12). Importantly, the normalized totals for the data we collected at UNM and the normalized totals for the data we collected at JSC were indistinguishable within analytical error, so all of the data was included in the present study. In order to make direct comparisons of melt compositions from individual experiments, we normalized the totals to 100% Tables S1-S10, but the raw data for apatite and glasses are provided in Tables S11-S12.

The quenched silicate melts from each of the experiments exhibited a range in average compositions (Table S1) with SiO_2 abundances ranging from 35.82 to 50.55 wt.% using volatile-free melt compositions after normalization to 100% totals (VFNT). The average FeO abundances were also consistently high and ranged from 17.36 to 27.74 wt.% FeO (VFNT), which is consistent with a ferrobasaltic (>14 wt.% FeO) melt composition. The average Mg#'s of these compositions were low and ranged from 18.9 to 36.9. The range in average melt compositions is similar to those reported in the apatite-melt partitioning experiments of McCubbin et al. (2015b). The average F and Cl abundances in melt from the experiments are reported in Table S1 and Table 3. Fluorine abundances from the quenched glasses in our experimental run products ranged from below detection to a maximum of 1.17 wt.% F, and the Cl abundances ranged from 0.28 to

This is a preprint, the final version is subject to change, of the American Mineralogist (MSA)
Cite as Authors (Year) Title. American Mineralogist, in press.
DOI: https://doi.org/10.2138/am-2018-6339

3.6 wt.% Cl (Table 3). The F abundances in the melt were all below detection in the three experiments that had a starting F:Cl ratio of 10:90 (i.e., Q1b.013, Q1b.014, and Q1b.015).

The quenched melt in five of the experiments (Q1b.002, Q1b.003, Q1b.006, Q1b.009, and Q1b.012) exhibit evidence of compositional variation in back scattered electron images (i.e., Figure 1b, d), and the glasses also display a large range in chemical composition. Although this observation may indicate that the melts did not fully homogenize during crystallization, diffuse boundaries between immiscible silicate liquids have been reported in previous experimental studies on SLI (Charlier and Grove 2012), so we evaluate the chemical composition of the melt endmembers to assess whether SLI occurred in these five experimental charges. The average melt compositions from the five experiments have large standard deviations (i.e., Table S1), so we evaluate compositional differences between the two melt phases in Tables S2-S6. The bulk composition of QUE 94201, as well as the P-enriched compositions used in the present study (Table 1), fall within the two-liquid field defined in previous studies on SLI (e.g., Charlier and Grove 2012; Charlier et al. 2011; Pernet-Fisher et al. 2014; Roedder 1978). The two melt phases in each of the five experimental charges were represented by an Si-rich endmember and an Si-poor endmember, consistent with other occurrences of SLI in natural and synthetic systems (e.g., Charlier and Grove 2012; Philpotts 1976, 1979; Roedder 1978; Roedder and Weiblen 1970; Shearer et al. 2001). Furthermore, the Si-poor composition was enriched in P and Fe relative to the Si-rich composition, and the Si-rich endmember was enriched in Al and Na (Tables S2-S6). These observed elemental distributions between melt compositions are evidence in support of SLI (Charlier and Grove 2012; Tollari et al. 2006).

The partitioning of elements between immiscible silicate melts can provide important insights into the distribution of volatiles in natural systems that undergo SLI. The Si-rich

This is a preprint, the final version is subject to change, of the American Mineralogist (MSA)
Cite as Authors (Year) Title. American Mineralogist, in press.
DOI: https://doi.org/10.2138/am-2018-6339

346 endmember was enriched in SiO_2, Al_2O_3, and Na_2O relative to the Si-poor endmember.
347 Additionally, the Si-rich endmember was depleted in TiO_2, FeO, MgO, CaO, P_2O_5, F, and Cl
348 relative to the Si-poor endmember (Tables S2–S6). The Mg#s of both liquids are
349 indistinguishable within uncertainty. Additionally, the average F/Cl ratio between the Si-rich
350 endmember and the Si-poor endmember is 1.12 ± 0.12, indicating that the F/Cl ratio between the
351 two liquids is essentially equal, although a slight preference of F over Cl in the Si-rich conjugate
352 liquid is possible (Table S2–S6). The $melt_{Si\text{-}rich}$-$melt_{Si\text{-}poor}$ partition coefficients for F range from
353 1.00 to 0.48 with an average value of 0.79 ± 0.14, and the $melt_{Si\text{-}rich}$-$melt_{Si\text{-}poor}$ partition
354 coefficients for Cl range from 0.92 to 0.41 with an average value of 0.72 ± 0.17 (computed on a
355 wt.% basis). The preference for F and Cl in the mafic conjugate liquids increases as a function of
356 the difference in SiO_2 content of the two conjugate liquids (Figure 2). The preference for F and
357 Cl in the mafic conjugate liquid in systems that undergo SLI was also reported by Lester et al.
358 (2013).

359 **Apatite-melt partitioning of F and Cl**

360 Numerous studies investigating apatite-melt partitioning of F and Cl have demonstrated
361 that simple Nernst-like partition coefficients exhibit substantial variation because F and Cl are
362 essential structural constituents in apatite (Boyce et al. 2014; Doherty et al. 2014; Li and
363 Hermann 2015, 2017; Mathez and Webster 2005; McCubbin et al. 2015b; Webster and Piccoli,
364 2015; Webster et al. 2009, 2017). This variation arises because the combined concentrations of F
365 and Cl in apatite are fixed (based on apatite stoichiometry) and the concentrations of F and Cl in
366 vapor-undersaturated silicate melts at apatite saturation are much less constrained (Boyce et al.
367 2014; McCubbin et al. 2015b). Moreover, the existence of apatite is predicated on a populated X-
368 site, but the existence of the melt is not predicated on halogen abundances. Nonetheless, many

This is a preprint, the final version is subject to change, of the American Mineralogist (MSA)
Cite as Authors (Year) Title. American Mineralogist, in press.
DOI: https://doi.org/10.2138/am-2018-6339

previous apatite-melt partitioning studies have reported Nernst-like partition coefficients, so we compute them as well to compare our results to previous studies and to demonstrate why they should not be used for computing melt abundances of halogens from apatite. The simple Nernst-like partition coefficients are computed according to the following:

$$D_X^{Ap-Melt} = \frac{X_{Ap}}{X_{Melt}} \quad (1)$$

where $D_X^{Ap-Melt}$ is the apatite-melt partition coefficient for component X, X_{Ap} is the concentration of X in apatite, and X_{Melt} is the concentration of X in the coexisting melt. Although D values exhibit substantial variability, recent studies have demonstrated that the D values for F and Cl exhibit predictable interdependence despite the large reported range in values. This interdependence was identified by examining exchange coefficients (i.e., ratios of mineral-melt D values) instead of Nernst-like partition coefficients (Eq. 1) (Boyce et al. 2014; Li and Hermann 2015, 2017; McCubbin et al. 2015b; Riker et al. 2018; Webster et al. 2017). Consequently, we report exchange coefficients in addition to D values to assess the partitioning behavior of F and Cl between apatite and silicate melt along the F-Cl apatite join. The Cl-F exchange equilibria is described in a general form by the reaction:

$$X_{Apatite} + Y_{Melt} \Leftrightarrow Y_{Apatite} + X_{Melt} \quad (2)$$

Here, $X_{Apatite}$ and $Y_{Apatite}$ represent the F and Cl endmember apatite components involved in the exchange reaction, respectively, and Y_{Melt} and X_{Melt} represent those same components in the silicate melt. At equilibrium, the equilibrium constant ($K_{Ap-Melt}^{Y-X}$) for this reaction can be expressed as:

$$K_{Ap-Melt}^{Y-X} = \frac{a_{Melt}^{X} \times a_{Apatite}^{Y}}{a_{Melt}^{Y} \times a_{Apatite}^{X}} \quad (3)$$

This is a preprint, the final version is subject to change, of the American Mineralogist (MSA)
Cite as Authors (Year) Title. American Mineralogist, in press.
DOI: https://doi.org/10.2138/am-2018-6339

where $a^{X}_{Apatite}$ and $a^{Y}_{Apatite}$ represent the activities of component X and Y, respectively, in apatite, and a^{X}_{Melt} and a^{Y}_{Melt} represent the activities of components X and Y, respectively, in the coexisting melt. This equilibrium constant can then be related to the partition coefficient (Eq. 1) as an exchange coefficient (K_d) (i.e., ratio of partition coefficients) according to the equation:

$$K_{d_{Y-X}}^{Ap-Melt} = \frac{X_{Melt} \times Y_{Ap}}{Y_{Melt} \times X_{Ap}} \quad (4)$$

Here, $K_{d_{Y-X}}^{Ap-Melt}$ is the apatite-melt exchange coefficient for components X and Y, X_{Melt} and Y_{Melt} are the concentrations of X and Y in the melt, respectively, and X_{Ap} and Y_{Ap} are the concentrations of X and Y in the apatite, respectively. As written (i.e., without activity coefficients), equation (4) includes an implicit assumption of ideality or that the ratios of the activity coefficients approach unity, which may not be valid. This approach to examining apatite-melt partitioning was described in detail by Boyce et al. (2014).

From the data in Table 3, we calculate a range of apatite-melt partition coefficients (using Eq. 1) for F (3–25) and Cl (0.5–2.5) (computed on a wt.% basis; Table 4). We were unable to compute apatite-melt partition coefficients for experiments Q1b.013, Q1b.014, and Q1b.015 because the F abundances of the melt in those experiments are below the detection limit of F by EPMA (i.e., ~300 ppm F for our UNM routine and ~1500 ppm for our JSC routine). The partition coefficients reported here indicate that F partitions more strongly into apatite than Cl in all of our experiments, and the D values are within the large range of values reported in previous studies (Boyce et al. 2014; Doherty et al. 2014; Li and Hermann 2015, 2017; Mathez and Webster 2005; McCubbin et al. 2015b; Webster and Piccoli 2015; Webster et al. 2009, 2017). The wide range in partition coefficients calculated using equation (1) from our data further demonstrates the importance of not using a single D value to determine volatile abundances in silicate melts from apatite.

This is a preprint, the final version is subject to change, of the American Mineralogist (MSA)
Cite as Authors (Year) Title. American Mineralogist, in press.
DOI: https://doi.org/10.2138/am-2018-6339

413 The exchange K_d (from Eq. 4) values from the present study are provided in Table 4 and
414 Tables S7–S10. Similar to the partition coefficients described above, we were unable to compute
415 exchange K_d values for experiments Q1b.013, Q1b.014, and Q1b.015 because the F abundances
416 of the melt in those experiments were below the detection limit. The values for $K_{d_{Cl-F}}^{Ap-Melt}$ range
417 from 0.08 to 0.21, with an average value of 0.14 ± 0.04 (Table 4). The computed $K_{d_{Cl-F}}^{Ap-Melt}$
418 values generally decrease with decreasing F abundance in apatite, decreasing F abundance in
419 silicate melt, increasing Cl abundance in apatite, and increasing Cl abundance in silicate melt
420 (Figure 3) for a given temperature. Additionally, $K_{d_{Cl-F}}^{Ap-Melt}$ values increase slightly with
421 increasing temperature, but this effect is subordinate to the apparent effect of F and Cl
422 abundances in apatite and melt (Figure 3). This temperature effect is best illustrated in apatites
423 with ≥0.94 sfu F (Figure 3a). In fact, the temperature effect on $K_{d_{Cl-F}}^{Ap-Melt}$ values between 950 °C
424 and 1000 °C for apatites with ≤0.88 sfu F appears to be absent (Figure 3a); however, the effect of
425 temperature on the partitioning behavior between 950 °C and 1000 °C for apatites with ≤0.88 sfu
426 F is apparent if only $K_{d_{Cl-F}}^{Ap-Melt}$ values with similar abundances of F in the melt are compared
427 (Figure 3c). The range in $K_{d_{Cl-F}}^{Ap-Melt}$ values and their apparent dependence on melt F abundance
428 indicate non-ideal behavior in the apatite-melt system under the conditions evaluated in the
429 present study. Notably, we do not observe intra-sample variations in $K_{d_{Cl-F}}^{Ap-Melt}$ values in
430 experiments that underwent SLI (Tables S7–S10). We analyzed several apatite-melt pairs in the
431 Si-rich and Si-poor regions of experiments that exhibited SLI (Table S7–S10), and there was no
432 detectable difference in $K_{d_{Cl-F}}^{Ap-Melt}$ values between apatite-melt pairs in the Si-rich region and
433 apatite-melt pairs in the Si-poor regions in any of the experimental run products.

434 **Discussion**

This is a preprint, the final version is subject to change, of the American Mineralogist (MSA)
Cite as Authors (Year) Title. American Mineralogist, in press.
DOI: https://doi.org/10.2138/am-2018-6339

Apatite-melt exchange coefficients for F and Cl can vary as a function of temperature, pressure, melt composition, apatite composition, and/or oxygen fugacity. In complex multi-component systems, it is often difficult to constrain how each of these parameters affects the observed values of the exchange coefficients. To better discern the effects of each of these parameters in the present study, we compare our results to those of our previous study on apatite-melt partitioning that utilized the same bulk starting materials as those used here. McCubbin et al. (2015b) evaluated apatite-melt partitioning of F, Cl, and OH in an H_2O-bearing system at 1.0–1.2 GPa, 950–1000 °C, and fO_2 in the range of ΔIW -1 to +2. In contrast to the results of the present study, the $K_{d_{Cl-F}}^{Ap-Melt}$ values reported in McCubbin et al. (2015b) exhibit less variation with an average value of 0.21 ± 0.03 (Figure 3). The primary differences between these two experimental studies include the pressure of crystallization and abundance of H_2O in the bulk starting composition, the latter of which translates to differences in apatite and melt compositions between the two studies. Consequently, we hypothesize that any major differences in partitioning behavior between the two studies can be attributed to either pressure effects or the abundance of H_2O in the system.

The effect of pressure on F-Cl exchange equilibria between apatite and melt

To assess the effect of pressure on $K_{d_{Cl-F}}^{Ap-Melt}$ values, we need to compare the results of experiments conducted at 0 GPa in the present study to experiments conducted at 1–1.2 GPa in McCubbin et al. (2015b). In order to independently assess the effect of pressure on the F-Cl exchange equilibria between apatite and melt in these two studies, we would need to disentangle the effects of all other parameters. Although we cannot avoid comparing an H_2O-rich melt in one system (i.e., McCubbin et al. 2015b) to an H_2O-poor melt in another system (i.e., this study), we can limit the range of temperatures to 950–1000 °C and limit apatite compositions to those that

This is a preprint, the final version is subject to change, of the American Mineralogist (MSA)
Cite as Authors (Year) Title. American Mineralogist, in press.
DOI: https://doi.org/10.2138/am-2018-6339

exhibit ideal mixing of anion components in the X-site to enable a more direct assessment of a pressure effect on $K_{d_{Cl-F}}^{Ap-Melt}$ values between both studies. Previously published solution calorimetry data indicate that apatites with >0.9 sfu F will exhibit ideal (or nearly ideal) mixing of F and Cl in apatite along the F-Cl binary (Hovis and Harlov 2010). Three of the experiments (Q1b.001, Q1b.002, and Q1b.003) from the present study produced apatites with sufficiently high F abundances. Two of the experiments with sufficiently fluorinated apatite (Q1b.002 and Q1b.003) were run in the temperature range of 950–1000 °C (Table 3). The average $K_{d_{Cl-F}}^{Ap-Melt}$ value for those two experiments is 0.17 ± 0.03. This $K_{d_{Cl-F}}^{Ap-Melt}$ value is slightly lower, with overlapping uncertainties, than the $K_{d_{Cl-F}}^{Ap-Melt}$ value at 1–1.2 GPa of 0.21 ± 0.03 (McCubbin et al. 2015b), indicating that there may be a minor positive pressure dependence on the $K_{d_{Cl-F}}^{Ap-Melt}$ values, although we caution that additional data is required to confirm this relationship because it was determined from an insufficient number of experiments at the low pressure end. Additionally, we cannot rule out that the minor difference in $K_{d_{Cl-F}}^{Ap-Melt}$ values can be attributed to differences in the abundances of H_2O in the silicate melt between the two studies. Although there may be a slight positive correlation between pressure and $K_{d_{Cl-F}}^{Ap-Melt}$ values, the observed pressure effect is too small to explain the large variation in $K_{d_{Cl-F}}^{Ap-Melt}$ values across the F-Cl apatite binary join in the present study. Consequently, we explore the role of melt and apatite composition on the observed variation in $K_{d_{Cl-F}}^{Ap-Melt}$ values.

The effect of composition on F-Cl exchange equilibria between apatite and melt

All of the apatites crystallized in the present study are nominally OH-free and hence lie along the F-Cl apatite binary join in F-Cl-OH apatite space (Figure 4). We chose to conduct apatite-melt partitioning experiments along this join based on solution calorimetry data that

This is a preprint, the final version is subject to change, of the American Mineralogist (MSA)
Cite as Authors (Year) Title. American Mineralogist, in press.
DOI: https://doi.org/10.2138/am-2018-6339

indicate F and Cl undergo non-ideal mixing along this join, with excess enthalpies of mixing as high as 8.3 kJ/mol (Hovis and Harlov 2010). We anticipated that non-ideal mixing of anion components in the apatite X-site would be manifest as variable $K_{d_{Cl-F}}^{Ap-Melt}$ values, as hypothesized in McCubbin et al. (2015b). In contrast, F and OH in F-rich apatite (> 0.6 sfu F) along the F-OH apatite binary join undergo ideal mixing (Hovis et al. 2014a), and we inferred from nearly invariant F-Cl-OH exchange equilibria between apatite and melt that F-rich apatites with ternary F-Cl-OH X-site compositions also undergo ideal mixing (McCubbin et al. 2015b). Although we confirmed in the present study that the $K_{d_{Cl-F}}^{Ap-Melt}$ values are variable when F and Cl mix non-ideally in apatite, the systematic behavior of how these values vary may provide important insights into the phenomenon that drives the variation.

The observed drop in $K_{d_{Cl-F}}^{Ap-Melt}$ values with decreasing F abundances in melt and apatite in the present study indicates that F becomes more compatible in apatite as there is less F in the system under the conditions investigated (i.e., 0 GPa, 950–1050 °C, anhydrous Fe-rich basaltic melt, and fO_2 at ~ΔIW -1). The range in $K_{d_{Cl-F}}^{Ap-Melt}$ values (0.08–0.21) and their apparent dependence on F abundance indicate non-ideal behavior in the apatite-melt system under these conditions. In contrast, the $K_{d_{Cl-F}}^{Ap-Melt}$ values reported in McCubbin et al. (2015b) exhibit minor variation with an average value of 0.21 ± 0.03 (Figure 3), indicating ideal behavior. The primary correlations observed in the variation of $K_{d_{Cl-F}}^{Ap-Melt}$ values in the present study are for F and Cl abundances in apatite and melt. However, the ranges of F and Cl abundances in apatite and melt from the H_2O-bearing apatite-melt partitioning experiments in McCubbin et al. (2015b) encompass the same range of F and Cl abundances in melt and apatite as those produced in the present study (Figure 3). Consequently, the abundances of F and Cl in melt and apatite, alone,

This is a preprint, the final version is subject to change, of the American Mineralogist (MSA)
Cite as Authors (Year) Title. American Mineralogist, in press.
DOI: https://doi.org/10.2138/am-2018-6339

cannot be the direct cause for the observed non-ideal behavior in $K_{d_{Cl-F}}^{Ap-Melt}$ values from the present study. This conclusion is not surprising given that we anticipate the differences in partitioning behavior between this study and our previous study (McCubbin et al. 2015b) to relate to either pressure effects or the abundance of H_2O in the system, and we have already ruled out the former as being the primary factor.

Low-OH apatites along or near the F-Cl binary join must create an off-mirror F site at (0,0,0.167) to maintain hexagonal symmetry in space group $P6_3/m$ (Hughes et al. 2014b). This off-mirror F position is coupled with a second Cl position at the adjacent mirror plane (0,0,0) away from the off-mirror F position (Hughes et al. 2014b). These two positions are in addition to the two typical anion positions for F and Cl in endmember fluorapatite and chlorapatite at (0,0,0.25) and (0,0,0.086), respectively (Hughes and Rakovan 2002; Hughes et al. 1989, 2014b). These four sites are required in F-Cl apatites to accommodate long-range Cl-F mixing in the apatite channels along the c-axis (Hughes et al. 2014b). However, at mole fractions of OH^- as low as 0.12 sfu in the apatite X-site, additional F and Cl positions to accommodate long-range Cl-F neighboring are not required (McCubbin et al. 2008). All of the Cl-bearing experiments from McCubbin et al. (2015b) had apatites with more than 0.12 sfu OH^-, and all of the experiments in the present study had apatite with less than 0.12 sfu OH^- (Table 3). Consequently, the low-OH^- apatites in the present study likely have a fundamentally different column anion arrangement than the OH^--rich apatites in the H_2O-bearing study of McCubbin et al. (2015b). Moreover, the observation in the present study that F becomes more compatible in apatite as there is less F in the system can be explained by the presence of the off-mirror F site in apatite that only F can occupy, which is required to stabilize the apatite structure in space group $P6_3/m$ (Hughes et al. 2014b). In fact, we speculate that the oxy component (i.e., O^{2-} + vacancy)

This is a preprint, the final version is subject to change, of the American Mineralogist (MSA)
Cite as Authors (Year) Title. American Mineralogist, in press.
DOI: https://doi.org/10.2138/am-2018-6339

525 substitution that appears in our F-poor experiments, and in other synthetic and natural systems
526 (Hovis and Harlov 2010; Jones et al. 2014, 2016; Schettler et al. 2011), may be a further result of
527 apatite structure stabilization in systems with a paucity of F and OH^- components to incorporate
528 into apatite.

529 We attribute the differences in $K_{d_{Cl-F}}^{Ap-Melt}$ values between our previous study and the
530 present study to the dissimilar H_2O abundances in the two sets of experiments. Specifically,
531 previous investigations into the atomic arrangements of F, Cl, and OH in apatite demonstrate that
532 the apatites from the H_2O-rich experiments of McCubbin et al. (2015b) exhibit steric
533 accommodations of F and Cl that are different from the apatites in the H_2O-poor experiments in
534 the present study (Hughes and Rakovan, 2002, 2015; Hughes et al. 1989, 1990, 2014b). The
535 steric controls on F and Cl in OH-poor apatites further elucidate the observed correlations
536 between variation of $K_{d_{Cl-F}}^{Ap-Melt}$ values with F and Cl abundances in apatite and melt from the
537 present study. These results demonstrate a causal link between atomic arrangements of apatite X-
538 site components, the thermodynamic mixing properties of apatite X-site components, and the
539 values of apatite-melt exchange equilibria for apatite X-site components.

540 **The effect of temperature on F-Cl exchange equilibria between apatite and melt**

541 To assess the effect of temperature on $K_{d_{Cl-F}}^{Ap-Melt}$ values, we need to limit apatite
542 compositions to those that exhibit ideal mixing of anion components in the X-site to enable a
543 more direct assessment of a temperature effect on $K_{d_{Cl-F}}^{Ap-Melt}$ values in the present study. As
544 discussed above, previously published solution calorimetry data indicate that apatites with >0.9
545 sfu F will exhibit ideal (or nearly ideal) mixing of F and Cl in apatite along the F-Cl binary
546 (Hovis and Harlov 2010). Three of the experiments (Q1b.001, Q1b.002, and Q1b.003) from the
547 present study produced apatites with sufficiently high F abundances. The apatite-melt exchange

This is a preprint, the final version is subject to change, of the American Mineralogist (MSA)
Cite as Authors (Year) Title. American Mineralogist, in press.
DOI: https://doi.org/10.2138/am-2018-6339

548 equilibria from these experiments exhibit a slight positive temperature dependence on $K_{d_{Cl-F}}^{Ap-Melt}$
549 values. A positive correlation between temperature and $K_{d_{Cl-F}}^{Ap-Melt}$ values has also been reported
550 in previous studies (Li and Hermann 2015, 2017). However, the temperature correlation is less
551 clear when the apatite compositions are within the region of non-ideal mixing of F and Cl in the
552 X-site (Figure 3).

553 **Effects of SLI on apatite compositions and apatite-melt partitioning of F and Cl**

554 The effect of silicate liquid immiscibility on the partitioning behavior of F, Cl, and OH
555 between apatite and silicate melt has not been determined previously. However, Pernet-Fisher et
556 al. (2014) reported that apatite-based melt hygrometry in lunar systems would be complicated by
557 the effects of SLI. In particular, they speculated that apatites crystallizing from each of the
558 respective conjugate liquids would be different, and they further postulated that the partitioning
559 behavior of F, Cl, and OH between apatite and melt would be different based on the differing
560 melt compositions of those conjugate liquids (Pernet-Fisher et al. 2014). The latter point has also
561 been raised in the context of whether one should consider only the melt compositions of late-
562 stage melt pockets from which apatite has crystallized to determine appropriate apatite-melt
563 exchange coefficients (Potts et al. 2016). Although we did not systematically investigate the
564 effect of SLI or melt composition on F-Cl exchange equilibria between apatite and melt, five of
565 our experiments exhibit evidence that they underwent SLI. Notably, our experiments cannot
566 directly address the concerns of apatite-based melt hygrometry raised by Pernet-Fisher et al.
567 (2014) because our experiments did not contain H_2O. Nonetheless, we can compare the apatite-
568 melt pairs in each of the conjugate liquids from the SLI experiments to search for any first-order
569 effects of SLI on apatite composition or the F and Cl partitioning behavior between apatite and
570 silicate melt.

This is a preprint, the final version is subject to change, of the American Mineralogist (MSA)
Cite as Authors (Year) Title. American Mineralogist, in press.
DOI: https://doi.org/10.2138/am-2018-6339

We analyzed several apatite-melt pairs in the Si-rich and Si-poor regions of our experiments that exhibited SLI (Table S7–S10). Our results indicate that F and Cl partition more strongly into the Si-poor conjugate liquid, demonstrating that the process of SLI can redistribute volatiles in natural systems. This observation is consistent with previous experimental work on F and Cl partitioning in systems that undergo SLI (Lester et al. 2013). Although F and Cl were not evenly distributed between the two conjugate liquids, our results indicate that the F/Cl ratio in the Si-poor liquids was similar to that of the Si-rich liquids (Table S7–S10). Moreover, the F and Cl abundances of apatite within the two conjugate liquids were indistinguishable, and we did not observe a bi-modal population of apatite compositions. Consequently, we did not observe detectable differences in computed $K_{d_{Cl-F}}^{Ap-Melt}$ values for apatite-melt pairs in either of the two conjugate liquids in each of the SLI experiments.

The initiation of silicate-liquid immiscibility is an equilibrium process that results in the presence of two melt phases in a single system. As long as those two melt phases remain in equilibrium throughout crystallization, each of the respective conjugate liquids will be in equilibrium with the solid assemblage that is crystallized, and the solid assemblage from one liquid will be in equilibrium with the solid assemblage of the other liquid. Given that there is no evidence of a miscibility gap within apatite F-Cl-OH ternary space at magmatic temperatures (e.g., Hovis and Harlov 2010; Hughes et al. 2014b), there should only be one apatite composition in equilibrium with both of the conjugate liquids. It is possible for the values of apatite-melt exchange coefficients for various anion pairs to change between the two conjugate liquids if the activity-composition relationships for those anions are different between the two melt compositions. However, the observation that the F:Cl ratio of the two conjugate liquids in our SLI experiments remained nearly the same is evidence that the relative activity-composition

This is a preprint, the final version is subject to change, of the American Mineralogist (MSA)
Cite as Authors (Year) Title. American Mineralogist, in press.
DOI: https://doi.org/10.2138/am-2018-6339

relationships for F and Cl were not different for the two liquids, which lends credence to the idea that F and Cl can be treated as Henrian trace elements in the silicate melt at the abundances of F and Cl that have been investigated in many apatite-melt partitioning studies to date (Li and Hermann 2015, 2017; McCubbin et al. 2015b; Webster et al. 2017).

In conclusion, SLI is not likely to be the cause for the observed intra-sample variation in apatite compositions from pockets of late-stage mesostasis in many lunar samples (c.f., Pernet-Fisher et al. 2014; Potts et al. 2016). Intra-sample variation in apatite compositions occurs in many natural samples, including samples that do not exhibit SLI. The observed variations in apatite X-site composition is better explained by processes such as fractional crystallization, assimilation, or magmatic degassing (Boyce and Hervig 2008, 2009; Boyce et al. 2014; Greenwood et al. 2011; McCubbin et al. 2011, 2013, 2016; Meurer and Boudreau 1996; Tartèse et al. 2013, 2014; Treiman et al. 2014; Ustunisik et al. 2011, 2015). However, an important distinction between the conditions of our experiments and those of the natural lunar system discussed by Pernet-Fisher (2014) is the absence of H_2O in our experiments. Consequently, before we can rule out entirely the possibility that SLI will have an effect on F-Cl-OH exchange equilibria between apatite and melt, H_2O-bearing apatite-saturated systems that exhibit SLI need to be investigated experimentally.

Application of apatite-melt exchange equilibria to natural OH-poor F-Cl apatites

Numerous studies have identified apatites in samples from numerous terrestrial bodies within the Solar System that exhibit X-site compositions that lie along or close to the F-Cl apatite binary join (e.g., Boudreau et al. 1995; Harlov et al. 2006; Hughes et al. 2014a; Jolliff et al. 1993; Jones et al. 2014, 2016; Lewis and Jones 2016; McCubbin and Nekvasil, 2008; McCubbin et al. 2015a; Patiño Douce and Roden 2006; Shearer et al. 2011; Treiman et al. 2014; White et al.

This is a preprint, the final version is subject to change, of the American Mineralogist (MSA)
Cite as Authors (Year) Title. American Mineralogist, in press.
DOI: https://doi.org/10.2138/am-2018-6339

2005). The Cl-depleted apatites near this join, with molar X-site occupancies of F > 0.9 sfu, could have formed from systems with H_2O, and they appear to exhibit F and Cl partitioning behavior between apatite and melt that is analogous to F-rich ternary F-Cl-OH apatites (McCubbin et al. 2015b). F-Cl apatites with less than 0.9 sfu F and less than 0.12 sfu OH exhibit non-ideal mixing of F and Cl in the apatite X-site that is accompanied by changes in the steric accommodation of F and Cl in the apatite X-site (Hovis and Harlov 2010; Hughes et al. 2014b; McCubbin et al. 2008). Moreover, these Cl-rich apatites (i.e., Cl > 0.1 sfu of apatite X-site) do not exhibit F and Cl partitioning behavior between apatite and melt that would be amenable to using these apatites to determine halogen abundances of silicate melts. In fact, the strong preference for F to stabilize the apatite structure likely applies to OH as well because OH also aids in stabilizing the structure of F-rich, Cl-bearing apatites (Hughes and Rakovan 2002; McCubbin et al. 2008). Consequently, we suggest that Cl-rich apatites (i.e., Cl > 0.1 sfu of apatite X-site) with compositions near the F-Cl binary join that formed from any H_2O-bearing natural systems should not be used for apatite-based melt-hygrometry. Based on the results of the present study, we have re-assessed the "forbidden" region within apatite F-Cl-OH ternary space where apatite compositions should not be used for melt-hygrometry (Figure 4). Importantly, and as we pointed out in our previous work (McCubbin et al. 2015b), even when apatites have X-site compositions that are amenable to using apatite for melt-hygrometry, apatite-melt exchange coefficients can also vary as a function of temperature, pressure, melt composition, and/or oxygen fugacity. Future efforts are needed to understand the effects of these parameters before we will have a widely applicable model for apatite-based melt hygrometry.

Implications

This is a preprint, the final version is subject to change, of the American Mineralogist (MSA)
Cite as Authors (Year) Title. American Mineralogist, in press.
DOI: https://doi.org/10.2138/am-2018-6339

639 The harmony between the structural accommodation mechanism of F and Cl in OH-poor
640 apatite, the thermodynamic mixing properties of F and Cl in OH-poor apatite, and the F and Cl
641 partitioning behavior between OH-poor melt and OH-poor apatite further demonstrates the
642 power of crystal chemistry in the development of mineralogical tools to solve petrologic
643 problems on Earth and beyond. Although this is the first experimental study to assess apatite-
644 melt exchange equilibria of X-site components along an apatite binary join, the two remaining
645 joins (F-OH and Cl-OH) represent additional opportunities to check for consistency among all
646 three datasets. Furthermore, the agreement between these datasets allows us to make predictions
647 that can be tested by future studies.

648 Solution calorimetry data from the F-OH apatite binary indicates that OH and F mix
649 ideally from the fluorapatite endmember until approximately F_{60}–OH_{40}, at which point apatite
650 exhibits negative enthalpies of F-OH mixing (Hovis et al. 2014a). Future studies can determine
651 whether there are changes in the steric accommodation of F and OH in the apatite structure that
652 correspond to this composition. Additionally, apatite-melt partitioning experiments could
653 demonstrate whether $K_{d_{OH-F}}^{Ap-Melt}$ values are constant between F_{60} and F_{100} and become variable
654 between OH_{40} and OH_{100}.

655 Crystallographic studies of apatite along the Cl-OH join have demonstrated three
656 different structural accommodation mechanisms of Cl and OH along this join that vary as a
657 function of apatite composition (Hughes et al. 2016). Specifically, apatites with more Cl than OH
658 have three column anion positions (two for Cl and one for OH), apatites with more OH than Cl
659 have three column anion positions (one for Cl, one for OH, and one that is shared between Cl
660 and OH), and apatites that have equal amounts of Cl and OH have four column anion positions
661 (one for Cl, two for OH, and one that is shared between Cl and OH). Given the structural

This is a preprint, the final version is subject to change, of the American Mineralogist (MSA)
Cite as Authors (Year) Title. American Mineralogist, in press.
DOI: https://doi.org/10.2138/am-2018-6339

662 complexities that exist along this binary apatite join, it is intriguing to think about how this
663 complexity is manifested in the thermodynamic mixing properties of OH and Cl in OH-Cl
664 apatite. The limited data that exist, that can assess the partitioning behavior of OH and Cl in an
665 F-depleted apatite-melt system, already hint that the partitioning behavior is complex compared
666 to ternary F-Cl-OH apatite (McCubbin et al. 2015b). However, assessing partitioning at each of
667 the structural transitions along the OH-Cl join will be very important for improving the Cl-rich
668 end of fractional crystallization models of apatite (i.e., McCubbin et al. 2016).

669 **Acknowledgements**

670 The authors are grateful for discussions with Kathleen Vander Kaaden, Jessica Barnes,
671 and Jeremy Boyce during the preparation of this manuscript. We are also thankful to David
672 Walker for his intellectual input and for providing laboratory facilities required for the
673 experiments to be completed successfully. FM and GU acknowledge support from the NASA
674 Cosmochemistry Program through a grant awarded to FM and a grant awarded to Denton Ebel
675 (NNX10AI42G), respectively. GU also acknowledges support from an AMNH Katherine Davis
676 postdoctoral fellowship during this study. The authors would like to thank Bradley Jolliff and
677 Philip Piccoli for detailed and thoughtful reviews that greatly helped to improve the quality and
678 clarity of the manuscript. The authors are also grateful to Daniel Harlov for the editorial
679 handling of this manuscript.

680 **References**

681 Boudreau A.E., Love C., and Prendergast M.D. (1995) Halogen geochemistry of the Great Dyke,
682 Zimbabwe. Contributions to Mineralogy and Petrology, 122, 289-300.
683 Boyce J.W. and Hervig R.L. (2008) Magmatic degassing histories from apatite volatile
684 stratigraphy. Geology, 36, 63-66.
685 Boyce J.W. and Hervig R.L. (2009) Apatite as a monitor of late-stage magmatic processes at
686 Volcán Irazú, Costa Rica. Contributions to Mineralogy and Petrology, 157, 135-145.

687 Boyce J.W., Liu Y., Rossman G.R., Guan Y., Eiler J.M., Stolper E.M., and Taylor L.A. (2010)
688 Lunar apatite with terrestrial volatile abundances. Nature, 466, 466-469.
689 Boyce J.W., Tomlinson S.M., McCubbin F.M., Greenwood J.P., and Treiman A.H. (2014) The
690 Lunar Apatite Paradox. Science, 344, 400-402.
691 Brenan J.M. (1993) Partitioning of fluorine and chlorine between apatite and aqueous fluids at
692 high-pressure and temperature: Implications for the F and Cl content of high P-T Fluids.
693 Earth and Planetary Science Letters, 117, 251-263.
694 Burnham C.W. (1994) Development of the Burnham model for prediction of H_2O solubility in
695 magmas. In M.R. Carroll and J.R. Holloway, Eds., Volatiles in Magmas, 30, p. 123-129.
696 Reviews in Mineralogy, Mineralogical Society of America, Washington, DC.
697 Candela P.A. (1986) Toward a thermodynamic model for the halogens in magmatic systems: An
698 application to melt vapor apatite equilibria. Chemical Geology, 57, 289-301.
699 Charlier B. and Grove T.L. (2012) Experiments on liquid immiscibility along tholeiitic liquid
700 lines of descent. Contributions to Mineralogy and Petrology, 164, 27-44.
701 Charlier B., Namur O., Toplis M.J., Schiano P., Cluzel N., Higgins M.D., and Vander Auwera J.
702 (2011) Large-scale silicate liquid immiscibility during differentiation of tholeiitic basalt
703 to granite and the origin of the Daly gap. Geology, 39, 907-910.
704 Doherty A.L., Webster J.D., Goldoff B.A., and Piccoli P.M. (2014) Partitioning behavior of
705 chlorine and fluorine in felsic melt-fluid(s)-apatite systems at 50 MPa and 850-950 °C.
706 Chemical Geology, 384, 94-111.
707 Filiberto J. and Dasgupta R. (2011) Fe^{2+}-Mg partitioning between olivine and basaltic melts:
708 Applications to genesis of olivine-phyric shergottites and conditions of melting in the
709 Martian interior. Earth and Planetary Science Letters, 304, 527-537.
710 Filiberto J., Gross J., and McCubbin F.M. (2016) Constraints on the water, chlorine, and fluorine
711 content of the Martian mantle. Meteoritics & Planetary Science, 51, 2023-2035.
712 Goldoff B., Webster J.D., and Harlov D.E. (2012) Characterization of fluor-chlorapatites by
713 electron probe microanalysis with a focus on time-dependent intensity variation of
714 halogens. American Mineralogist, 97, 1103-1115.
715 Greenwood J.P., Itoh S., Sakamoto N., Warren P., Taylor L., and Yurimoto H. (2011) Hydrogen
716 isotope ratios in lunar rocks indicate delivery of cometary water to the Moon. Nature
717 Geoscience, 4, 79-82.

718 Gross J., Filiberto J., and Bell A.S. (2013) Water in the martian interior: Evidence for terrestrial
719 MORB mantle-like volatile contents from hydroxyl-rich apatite in olivine–phyric
720 shergottite NWA 6234. Earth and Planetary Science Letters, 369–370, 120-128.
721 Harlov D., Renzulli A., and Ridolfi F. (2006) Iron-bearing chlor-fluorapatites in crustal xenoliths
722 from the Stromboli volcano (Aeolian Islands, Southern Italy): An indicator of fluid
723 processes during contact metamorphism. European Journal of Mineralogy, 18, 233-241.
724 Harlov D.E. (2015) Apatite: A fingerprint for metasomatic processes. Elements, 11, 171-176.
725 Harrison T.M. and Watson E.B. (1984) The behavior of apatite during crustal anatexis:
726 Equilibrium and kinetic considerations. Geochimica et Cosmochimica Acta, 48, 1467-
727 1477.
728 Holzheid A., Borisov A., and Palme H. (1994) The effect of oxygen fugacity and temperature on
729 solubilities of nickel, cobalt, and molybdenum in silicate melts. Geochimica et
730 Cosmochimica Acta, 58, 1975-1981.
731 Hovis G.L. and Harlov D.E. (2010) Solution calorimetric investigation of fluor-chlorapatite
732 crystalline solutions. American Mineralogist, 95, 946-952.
733 Hovis G.L., McCubbin F.M., Nekvasil H., Ustunisik G., Woerner W.R., and Lindsley D.H.
734 (2014a) A novel technique for fluorapatite synthesis and the thermodynamic mixing
735 behavior of F-OH apatite crystalline solutions. American Mineralogist, 99, 890-897.
736 Hovis G.L., Scott B.T., Altomare C.M., Leaman A.R., Morris M.D., Tomaino G.P., and
737 McCubbin F.M. (2014b) Thermal expansion of fluorapatite-hydroxylapatite crystalline
738 solutions. American Mineralogist, 99, 2171-2175.
739 Hughes J.M., Cameron M., and Crowley K.D. (1989) Structural variations in natural F, OH, and
740 Cl apatites. American Mineralogist, 74, 870-876.
741 Hughes J.M., Cameron M., and Crowley K.D. (1990) Crystal-structures of natural ternary
742 apatites: Solid-solution in the $Ca_5(PO_4)_3X$ (X= F, OH, Cl) system. American
743 Mineralogist, 75, 295-304.
744 Hughes J.M., Harlov D., Kelly S.R., Rakovan J., and Wilke M. (2016) Solid solution in the
745 apatite OH-Cl binary system: compositional dependence of solid solution mechanisms in
746 calcium phosphate apatites along the Cl-OH binary. American Mineralogist, 101, 1783-
747 1791.

748 Hughes J.M., Heffernan K.M., Goldoff B., and Nekvasil H. (2014a) Cl-rich fluorapatite, devoid
749 of OH, from the Three Peaks area, Utah: The first reported structure of natural Cl-rich
750 fluorapatite. Canadian Mineralogist, 52, 643-651.
751 Hughes J.M., Nekvasil H., Ustunisik G., Lindsley D.H., Craraor A.E., Vaughn J., Phillips B.L.,
752 McCubbin F.M., and Woerner W.R. (2014b) Solid solution in the fluorapatite-
753 chlorapatite binary system: High-precision crystal structure refinements of synthetic F-Cl
754 apatite. American Mineralogist, 99, 369-376.
755 Hughes J.M. and Rakovan J. (2002) The crystal structure of apatite, $Ca_5(PO_4)_3(F,OH,Cl)$. In
756 M.J. Kohn, J. Rakovan, and J.M. Hughes, Eds., Phosphates: Geochemical, Geobiological,
757 and Materials Importance, 48, p. 1-12. Reviews in Mineralogy and Geochemistry,
758 Mineralogical Society of America, Washington, DC.
759 Hughes J.M. and Rakovan J.F. (2015) Structurally robust, chemically diverse: Apatite and
760 apatite supergroup minerals. Elements, 11, 165-170.
761 Jarosewich E., Nelen J.A., and Norberg J.A. (1980) Reference samples for electron microprobe
762 analysis. Geostandards Newsletter, 4, 43-47.
763 Jolliff B.L., Haskin L.A., Colson R.O., and Wadhwa M. (1993) Partitioning in REE-saturating
764 minerals: Theory, experiment, and modeling of whitlockite, apatite, and evolution of
765 lunar residual magmas. Geochimica et Cosmochimica Acta, 57, 4069-4094.
766 Jones R.H., McCubbin F.M., Dreeland L., Guan Y.B., Burger P.V., and Shearer C.K. (2014)
767 Phosphate minerals in LL chondrites: A record of the action of fluids during
768 metamorphism on ordinary chondrite parent bodies. Geochimica et Cosmochimica Acta,
769 132, 120-140.
770 Jones R.H., McCubbin F.M., and Guan Y. (2016) Phosphate minerals in the H group of ordinary
771 chondrites, and fluid activity recorded by apatite heterogeneity in the Zag H3-6 regolith
772 breccia. American Mineralogist, 101, 2452-2467.
773 Korzhinskiy M.A. (1981) Apatite solid solutions as indicators of the fugacity of HCl and HF in
774 hydrothermal fluids. Geochemistry International, 3, 44-60.
775 Kring D.A., Gleason J.D., Swindle T.D., Nishiizumi K., Caffee M.W., Hill D.H., Jull A.J.T., and
776 Boynton W.V. (2003) Composition of the first bulk melt sample from a volcanic region
777 of Mars: Queen Alexandra Range 94201. Meteoritics & Planetary Science 38, 1833-
778 1848.

779 Lester G.W., Clark A.H., Kyser T.K., and Naslund H.R. (2013) Experiments on liquid
780 immiscibility in silicate melts with H_2O, P, S, F and Cl: Implications for natural magmas.
781 Contributions to Mineralogy and Petrology, 166, 329-349.
782 Lewis J.A. and Jones R.H. (2016) Phosphate and feldspar mineralogy of equilibrated L
783 chondrites: The record of metasomatism during metamorphism in ordinary chondrite
784 parent bodies. Meteoritics & Planetary Science, 51, 1886-1913.
785 Li H. and Hermann J. (2015) Apatite as an indicator of fluid salinity: An experimental study of
786 chlorine and fluorine partitioning in subducted sediments. Geochimica et Cosmochimica
787 Acta, 166, 267-297.
788 Li H.J. and Hermann J. (2017) Chlorine and fluorine partitioning between apatite and sediment
789 melt at 2.5 GPa, 800 ^{o}C: A new experimentally derived thermodynamic model. American
790 Mineralogist, 102, 580-594.
791 Mason H.E., McCubbin F.M., Smirnov A., and Phillips B.L. (2009) Solid-state NMR and IR
792 spectroscopic investigation of the role of structural water and F in carbonate-rich
793 fluorapatite. American Mineralogist, 94, 507-516.
794 Mathez E.A. and Webster J.D. (2005) Partitioning behavior of chlorine and fluorine in the
795 system apatite-silicate melt-fluid. Geochimica et Cosmochimica Acta, 69, 1275-1286.
796 McCubbin F.M., Boyce J.W., Srinivasan P., Santos A.R., Elardo S.M., Filiberto J., Steele A., and
797 Shearer C.K. (2016) Heterogeneous distribution of H_2O in the martian interior:
798 Implications for the abundance of H_2O in depleted and enriched mantle sources.
799 Meteoritics & Planetary Science, 51, 2036-2060.
800 McCubbin F.M., Elardo S.M., Shearer C.K., Smirnov A., Hauri E.H., and Draper D.S. (2013) A
801 petrogenetic model for the co-magmatic origin of chassignites and nakhlites: Inferences
802 from chlorine-rich minerals, petrology, and geochemistry. Meteoritics & Planetary
803 Science, 48, 819-853.
804 McCubbin F.M., Hauri E.H., Elardo S.M., Vander Kaaden K.E., Wang J., and Shearer C.K.
805 (2012) Hydrous melting of the martian mantle produced both depleted and enriched
806 shergottites. Geology, 40, 683-686.
807 McCubbin F.M., Jolliff B.L., Nekvasil H., Carpenter P.K., Zeigler R.A., Steele A., Elardo S.M.,
808 and Lindsley D.H. (2011) Fluorine and chlorine abundances in lunar apatite: Implications

809 for heterogeneous distributions of magmatic volatiles in the lunar interior. Geochimica et
810 Cosmochimica Acta, 75, 5073-5093.
811 McCubbin F.M. and Jones R.H. (2015) Extraterrestrial spatite: Planetary geochemistry to
812 astrobiology. Elements, 11, 183-188.
813 McCubbin F.M., Vander Kaaden K.E., Tartèse R., Klima R.L., Liu Y., Mortimer J., Barnes J.J.,
814 Shearer C.K., Treiman A.H., Lawrence D.J., Elardo S.M., Hurley D.M., Boyce J.W., and
815 Anand M. (2015a) Magmatic volatiles (H, C, N, F, S, Cl) in the lunar mantle, crust, and
816 regolith: Abundances, distributions, processes, and reservoirs. American Mineralogist,
817 100, 1668-1707.
818 McCubbin F.M., Mason H.E., Park H., Phillips B.L., Parise J.B., Nekvasil H., and Lindsley D.H.
819 (2008) Synthesis and characterization of low-OH- fluor-chlorapatite: A single crystal
820 XRD and NMR spectroscopic study. American Mineralogist, 93, 210-216.
821 McCubbin F.M. and Nekvasil H. (2008) Maskelynite-hosted apatite in the Chassigny meteorite:
822 Insights into late-stage magmatic volatile evolution in martian magmas. American
823 Mineralogist, 93, 676-684.
824 McCubbin F.M., Steele A., Hauri E.H., Nekvasil H., Yamashita S., and Hemley R.J. (2010a)
825 Nominally hydrous magmatism on the Moon. Proceedings of the National Academy of
826 Sciences of the United States of America, 27, 11223-11228.
827 McCubbin F.M., Steele A., Nekvasil H., Schnieders A., Rose T., Fries M., Carpenter P.K., and
828 Jolliff B.L. (2010b) Detection of structurally bound hydroxyl in fluorapatite from Apollo
829 mare basalt 15058,128 using TOF-SIMS. American Mineralogist, 95, 1141-1150.
830 McCubbin F.M., Tosca N.J., Smirnov A., Nekvasil H., Steele A., Fries M., and Lindsley D.H.
831 (2009) Hydrothermal jarosite and hematite in a pyroxene-hosted melt inclusion in
832 martian meteorite Miller Range (MIL) 03346: Implications for magmatic-hydrothermal
833 fluids on Mars. Geochimica et Cosmochimica Acta, 73, 4907-4917.
834 McCubbin F.M., Vander Kaaden K.E., Tartèse R., Boyce J.W., Mikhail S., Whitson E.S., Bell
835 A.S., Anand M., Franchi I.A., Wang J.H., and Hauri E.H. (2015b) Experimental
836 investigation of F, Cl, and OH partitioning between apatite and Fe-rich basaltic melt at
837 1.0-1.2 GPa and 950-1000 ^{o}C. American Mineralogist, 100, 1790-1802.

838 Meurer W.P. and Boudreau A.E. (1996) An evaluation of models of apatite compositional
839 variability using apatite from the middle banded series of the Stillwater Complex,
840 Montana. Contributions to Mineralogy and Petrology, 125, 225-236.
841 Newcombe M.E., Brett A., Beckett J.R., Baker M.B., Newman S., Guan Y., Eiler J.M., and
842 Stolper E.M. (2017) Solubility of water in lunar basalt at low pH_2O. Geochimica et
843 Cosmochimica Acta, 200, 330-352.
844 O'Neill H.S. and Pownceby M.I. (1993) Thermodynamic data from redox reactions at high
845 temperatures Part 1: An experimental and theoretical assessment of the electrochemical
846 method using stabalized zirconia electrolytes, with revised values for the Fe-FeO, Co-
847 CoO, Ni-NiO, and Cu-Cu_2O oxygen buffers and new data for the W-WO_2 buffer.
848 Contributions to Mineralogy and Petrology, 114, 296-314.
849 O'Neill H.S.C. (1986) Mo-MoO_2 (MOM) oxygen buffer and the free energy of formation of
850 MoO_2. American Mineralogist, 71, 1007-1010.
851 Pan Y.M. and Fleet M.E. (2002) Compositions of the apatite-group minerals: Substitution
852 mechanisms and controlling factors. In M.J. Kohn, J. Rakovan, and J.M. Hughes, Eds.,
853 Phosphates: Geochemical, Geobiological, and Materials Importance, 48, p. 13-49.
854 Reviews in Mineralogy and Geochemistry, Mineralogical Society of America,
855 Washington, DC.
856 Patiño Douce A.E. and Roden M.F. (2006) Apatite as a probe of halogen and water fugacities in
857 the terrestrial planets. Geochimica et Cosmochimica Acta, 70, 3173-3196.
858 Patiño Douce A.E., Roden M.F., Chaumba J., Fleisher C., and Yogodzinski G. (2011)
859 Compositional variability of terrestrial mantle apatites, thermodynamic modeling of
860 apatite volatile contents, and the halogen and water budgets of planetary mantles.
861 Chemical Geology, 288, 14-31.
862 Pernet-Fisher J.F., Howarth G.H., Liu Y., Chen Y., and Taylor L.A. (2014) Estimating the lunar
863 mantle water budget from phosphates: Complications associated with silicate-liquid-
864 immiscibility. Geochimica et Cosmochimica Acta, 144, 326-341.
865 Philpotts A.R. (1976) Silicate liquid immiscibility: Its probable extent and petrogenetic
866 significance. American Journal of Science, 276, 1147-1177.
867 Philpotts A.R. (1979) Silicate liquid immiscibility in tholeiitic basalts. Journal of Petrology, 20,
868 99-118.

869 Piccoli P. and Candela P. (1994) Apatite in felsic rocks: A model for the estimation of initial
870 halogen concentrations in the Bishop Tuff (Long Valley) and Tuolumne intrusive suite
871 (Sierra-Nevada Batholith) magmas. American Journal of Science, 294, 92-135.
872 Piccoli P.M. and Candela P.A. (2002) Apatite in igneous systems. In M.J. Kohn, J. Rakovan,
873 and J.M. Hughes, Eds., Phosphates: Geochemical, Geobiological, and Materials
874 Importance, 48, p. 255-292. Reviews in Mineralogy and Geochemistry, Mineralogical
875 Society of America, Washington, DC.
876 Potts N.J., Tartèse R., Anand M., van Westrenen W., Griffiths A.A., Barrett T.J., and Franchi
877 I.A. (2016) Characterization of mesostasis regions in lunar basalts: Understanding late-
878 stage melt evolution and its influence on apatite formation. Meteoritics & Planetary
879 Science, 51, 1555-1575.
880 Riker J., Humphreys M.C.S., Brooker R.A., De Hoog J.C.M., and EIMF (2018) First
881 measurements of OH-C exchange and temperature-dependent partitioning of OH and
882 halogens in the system apatite – silicate melt. American Mineralogist, 103, 260-270.
883 Roedder E. (1978) Silicate liquid immiscibility in magmas and in the system K_2O-FeO-Al_2O_3-
884 SiO_2: Example of serendipity. Geochimica et Cosmochimica Acta, 42, 1597-1617.
885 Roedder E. and Weiblen P.W. (1970) Silicate liquid immiscibility in lunar magmas, evidenced
886 by melt inclusions in lunar rocks. Science, 167, 641-644.
887 Roeder P.L. and Emslie R.F. (1970) Olivine-liquid equilibrium. Contributions to Mineralogy and
888 Petrology, 29, 275-289.
889 Sarafian A.R., Roden M.F., and Patiño Douce A.E. (2013) The volatile content of Vesta: Clues
890 from apatite in eucrites. Meteoritics & Planetary Science, 48, 2135-2154.
891 Schettler G., Gottschalk M., and Harlov D.E. (2011) A new semi-micro wet chemical method for
892 apatite analysis and its application to the crystal chemistry of fluorapatite-chlorapatite
893 solid solutions. American Mineralogist, 96, 138-152.
894 Sharp Z.D., Helffrich G.R., Bohlen S.R., and Essene E.J. (1989) The stability of sodalite in the
895 system $NaAlSiO_4$-NaCl. Geochimica et Cosmochimica Acta, 53, 1943-1954.
896 Shearer C.K., Burger P.V., Papike J.J., Sharp Z.D., and McKeegan K.D. (2011) Fluids on
897 differentiated asteroids: Evidence from phosphates in differentiated meteorites GRA
898 06128 and GRA 06129. Meteoritics & Planetary Science, 46, 1345-1362.

899 Shearer C.K., Papike J.J., and Spilde M.N. (2001) Trace-element partitioning between
900 immiscible lunar melts: An example from naturally occurring lunar melt inclusions.
901 American Mineralogist, 86, 238-246.
902 Shemesh A. (1990) Crystallinity and diagenesis of sedimentary apatites. Geochimica et
903 Cosmochimica Acta, 54, 2433-2438.
904 Stormer J.C., Pierson M.L., and Tacker R.C. (1993) Variation of F-X-ray and Cl-X-ray intensity
905 due to anisotropic diffusion in apatite during electron-microprobe analysis. American
906 Mineralogist, 78, 641-648.
907 Tacker R.C. and Stormer J.C. (1989) A thermodynamic model for apatite solid-solutions,
908 applicable to high-temperature geologic problems. American Mineralogist, 74, 877-888.
909 Tacker R.C. and Stormer J.C. (1993) Thermodynamics of Mixing of Liquids in the System
910 $Ca_3(PO_4)_2$-$CaCl_2$-CaF_2-$Ca(OH)_2$. Geochimica et Cosmochimica Acta, 57, 4663-4676.
911 Tartèse R., Anand M., Barnes J.J., Starkey N.A., Franchi I.A., and Sano Y. (2013) The
912 abundance, distribution, and isotopic composition of hydrogen in the Moon as revealed
913 by basaltic lunar samples: Implications for the volatile inventory of the Moon.
914 Geochimica et Cosmochimica Acta, 122, 58-74.
915 Tartèse R., Anand M., McCubbin F.M., Elardo S.M., Shearer C.K., and Franchi I.A. (2014)
916 Apatites in lunar KREEP basalts: The missing link to understanding the H isotope
917 systematics of the Moon. Geology, 42, 363-366.
918 Tollari N., Toplis M.J., and Barnes S.J. (2006) Predicting phosphate saturation in silicate
919 magmas: An experimental study of the effects of melt composition and temperature.
920 Geochimica et Cosmochimica Acta, 70, 1518-1536.
921 Toplis M.J. (2005) The thermodynamics of iron and magnesium partitioning between olivine and
922 liquid: Criteria for assessing and predicting equilibrium in natural and experimental
923 systems. Contributions to Mineralogy and Petrology, 149, 22-39.
924 Treiman A.H., Boyce J.W., Gross J., Guan Y.B., Eiler J.M., and Stolper E.M. (2014) Phosphate-
925 halogen metasomatism of lunar granulite 79215: Impact-induced fractionation of
926 volatiles and incompatible elements. American Mineralogist, 99, 1860-1870.
927 Ustunisik G., Nekvasil H., and Lindsley D.H. (2011) Differential degassing of H_2O, Cl, F, and S:
928 Potential effects on lunar apatite. American Mineralogist, 96, 1650-1653.

929 Ustunisik G., Nekvasil H., Lindsley D.H., and McCubbin F.M. (2015) Degassing pathways of
930 Cl-, F-, H-, and S-bearing magmas near the lunar surface: Implications for the
931 composition and Cl isotopic values of lunar apatite. American Mineralogist, 100, 1717-
932 1727.
933 Webster J.D., Goldoff B.A., Flesch R.N., Nadeau P.A., and Silbert Z.W. (2017) Hydroxyl, Cl,
934 and F partitioning between high-silica rhyolitic melts-apatite-fluid(s) at 50-200 MPa and
935 700-1000 °C. American Mineralogist, 102, 61-74.
936 Webster J.D. and Piccoli P.M. (2015) Magmatic apatite: A powerful, yet deceptive, mineral.
937 Elements, 11, 177-182.
938 Webster J.D., Tappen C.M., and Mandeville C.W. (2009) Partitioning behavior of chlorine and
939 fluorine in the system apatite-melt-fluid. II: Felsic silicate systems at 200 MPa.
940 Geochimica et Cosmochimica Acta, 73, 559-581.
941 White T., Ferraris C., Kim J., and Madhavi S. (2005) Apatite - An adaptive framework structure.
942 In G. Ferraris and S. Merlino, Eds., Micro- and Mesoporous Mineral Phases, 57, p. 307-
943 401. Reviews in Mineralogy and Geochemistry, Mineralogical Society of America,
944 Washington, DC.
945 Zhu C. and Sverjensky D.A. (1991) Partitioning of F-Cl-OH between minerals and hydrothermal
946 fluids. Geochimica et Cosmochimica Acta, 55, 1837-1858.

947

948

949 **Tables**

950

This is a preprint, the final version is subject to change, of the American Mineralogist (MSA)
Cite as Authors (Year) Title. American Mineralogist, in press.
DOI: https://doi.org/10.2138/am-2018-6339

Table 1: QUE 94201 meteorite composition from Kring et al. (2003) as well as compositions of F and Cl endmember powdered mixtures of QUE 94201 with added P. Compositions of powdered starting materials from McCubbin et al. (2015b).

Oxide (wt.%)	**QUE 94201**[a]	**QUE 94201 F Mixture**[b]	**QUE 94201 Cl Mixture**[b]
SiO_2	47.03	45.46	45.95
TiO_2	1.84	1.43	1.55
Al_2O_3	11.1	11.11	11.45
Cr_2O_3	0.14	0.14	0.14
FeO*	18.5	17.16	17.00
MnO	0.45	0.41	0.33
MgO	6.1	5.62	4.98
CaO	11.1	8.84	8.65
Na_2O	1.64	1.37	1.01
K_2O	0.05	-	-
P_2O_5	2.05	7.87	7.93
F	-	1.01	0.02
Cl	-	0.01	1.29
-O = F+ Cl	-	0.43	0.30
Total	100.00	100.00	100.00
mg#[c]	0.37	0.39	0.37

[a]QUE 94201 composition from Kring et al. (2003)
[b]Anhydrous compositions from McCubbin et al. (2015b)
[c]mg# = Molar Mg/(Mg + Fe^{2+}) assuming an $Fe^{2+}/\sum Fe = 0.9$.
*All Fe measured as FeO

Table 2: Experiments and experimental run conditions from the present study

This is a preprint, the final version is subject to change, of the American Mineralogist (MSA)
Cite as Authors (Year) Title. American Mineralogist, in press.
DOI: https://doi.org/10.2138/am-2018-6339

Exp. #	Capsule[a]	T (°C)	P (GPa)	Duration (hours)	Mixture type[b]	Phases[c]
Q1b.001	Mo	1050	0	8	90% F, 10% Cl	M, A, S
Q1b.002	Mo	1000	0	8	90% F, 10% Cl	M_D, M_L, A, P, S
Q1b.003	Mo	950	0	8	90% F, 10% Cl	M_D, M_L, A, P, I, S, Pl
Q1b.004	Mo	1050	0	8	75% F, 25% Cl	M, A, S
Q1b.005	Mo	1000	0	8	75% F, 25% Cl	M, A, P, S
Q1b.006	Mo	950	0	8	75% F, 25% Cl	M_D, M_L, A, P, I, S
Q1b.007	Mo	1050	0	8	50% F, 50% Cl	M, A, S
Q1b.008	Mo	1000	0	8	50% F, 50% Cl	M, A, P, S
Q1b.009	Mo	950	0	8	50% F, 50% Cl	M_D, M_L, A, P, I, S, H
Q1b.010	Mo	1050	0	8	25% F, 75% Cl	M, A, S
Q1b.012	Mo	950	0	8	25% F, 75% Cl	M_D, M_L, A, P, I, S, Pl
Q1b.013	Mo	1050	0	8	10% F, 90% Cl	M, A, S
Q1b.014	Mo	1000	0	8	10% F, 90% Cl	M, A, P, S
Q1b.015	Mo	950	0	8	10% F, 90% Cl	M, A, P, S

[a]Mo – molybdenum metal
[b] F – QUE 94201 F mixture, Cl – QUE 94201 Cl mixture (Table 1)
[c] M – melt (SLI conjugate liquids indicated by M_D and M_L), A – apatite, P – pyroxene, S – silica, I – ilmenite, Pl – plagioclase, H –Hercynitic spinel

964
965
966
967
968
969
970
971
972
973
974
975
976
977
978
979
980
981
982
983
984
985
986

Table 3: Volatile abundances of apatite and co-existing melt from experiments.

Exp. #	F_{melt}	F_{Ap}	Cl_{melt}	Cl_{Ap}	X_F	X_{Cl}	X_{other}[b]	$\sum X$

This is a preprint, the final version is subject to change, of the American Mineralogist (MSA)
Cite as Authors (Year) Title. American Mineralogist, in press.
DOI: https://doi.org/10.2138/am-2018-6339

Q1b.001	0.66 (2)	3.62 (7)	0.21 (1)	0.24 (2)	0.96 (2)	0.03 (0)	0.01 (2)	1.00
Q1b.002	0.61 (4)	3.53 (9)	0.31 (2)	0.32 (3)	0.94 (4)	0.05 (1)	0.03 (3)	1.02
Q1b.003	1.17 (18)	3.56 (9)	0.57 (10)	0.29 (1)	0.95 (3)	0.04 (0)	0.01 (3)	1.00
Q1b.004[a]	0.44 (4)	3.20 (3)	0.81 (2)	1.06 (5)	0.85 (1)	0.15 (1)	0.00 (0)	1.00
Q1b.005[a]	0.32 (4)	3.29 (4)	0.67 (3)	0.89 (4)	0.87 (1)	0.13 (1)	0.00 (0)	1.00
Q1b.006[a]	0.55 (6)	3.32 (1)	1.13 (18)	0.88 (1)	0.875 (0)	0.125 (0)	0.00 (0)	1.00
Q1b.007	0.25 (2)	2.58 (7)	1.24 (3)	2.03 (5)	0.70 (3)	0.29 (1)	0.02 (3)	1.01
Q1b.008	0.10 (2)	2.41 (8)	1.04 (4)	2.25 (11)	0.65 (3)	0.32 (2)	0.03 (3)	1.00
Q1b.009	0.19 (4)	2.44 (16)	2.11 (17)	2.35 (16)	0.65 (4)	0.33 (2)	0.02 (2)	1.00
Q1b.010	0.07 (1)	1.19 (11)	1.78 (3)	3.91 (7)	0.32 (3)	0.56 (1)	0.12 (4)	1.00
Q1b.012	0.13 (3)	1.49 (9)	4.0 (1.2)	3.59 (3)	0.41 (3)	0.52 (0)	0.07 (2)	1.00
Q1b.013	b.d.	0.56 (4)	1.99 (7)	5.00 (13)	0.15 (1)	0.73 (2)	0.12 (3)	1.00
Q1b.014	b.d.	0.28 (4)	2.33 (5)	5.69 (24)	0.08 (1)	0.82 (4)	0.10 (5)	1.00
Q1b.015	b.d.	0.30 (1)	3.06 (8)	5.52 (16)	0.08 (0)	0.79 (2)	0.13 (2)	1.00

Average abundances reported in wt.% from Table S1, which were normalized to 100% to enable direct comparison of values.
Parenthetical values represent 1σ SDOM and are always larger than the 2σ AU.
[a]F + Cl > 1 sfu, so F was calculated assuming $1 - X_{Cl} = X_F$.
[b]Value estimated by stoichiometry assuming $X_{other} = 1 - X_F - X_{Cl}$.
b.d. – analysis resulted in a value that was below analytical detection

Table 4: Apatite-melt partition coefficients and exchange

This is a preprint, the final version is subject to change, of the American Mineralogist (MSA)
Cite as Authors (Year) Title. American Mineralogist, in press.
DOI: https://doi.org/10.2138/am-2018-6339

coefficients.

Exp. #	$D_F^{Ap-Melt}$	$D_{Cl}^{Ap-Melt}$	$K_{d_{Cl-F}}^{Ap-Melt}$
Q1b.001	5.50 (22)	1.14 (12)	0.207 (24)
Q1b.002	5.74 (37)	1.01 (12)	0.176 (23)
Q1b.003	3.03 (48)	0.51 (9)	0.167 (40)
Q1b.003[a]	3.18 (35)	0.52 (6)	0.163 (10)
Q1b.004	7.23 (65)	1.31 (6)	0.181 (19)
Q1b.005	10.3 (1.2)	1.32 (8)	0.128 (17)
Q1b.006	5.99 (66)	0.78 (13)	0.130 (26)
Q1b.006[a]	5.43 (51)	0.73 (5)	0.136 (18)
Q1b.007	10.3 (1.0)	1.64 (6)	0.159 (17)
Q1b.008	25.3 (4.7)	2.16 (14)	0.085 (17)
Q1b.009	12.8 (2.7)	1.11 (12)	0.087 (20)
Q1b.009[a]	10.4 (1.3)	1.08 (2)	0.105 (13)
Q1b.010	16.4 (3.6)	2.19 (5)	0.134 (29)
Q1b.012	11.1 (2.8)	0.90 (27)	0.081 (32)
Q1b.012[a]	11.5 (2.6)	0.83 (25)	0.072 (8)
Q1b.013	-	2.52 (11)	-
Q1b.014	-	2.44 (12)	-
Q1b.015	-	1.80 (7)	-
Average 1050°C[b]	9.9 (4.8)	1.8 (6)	0.170 (31)
Average 1000°C[b]	14 (10)	1.7 (7)	0.130 (46)
Average 950°C[b]	8.2 (4.5)	1.0 (5)	0.116 (40)
Average All T°C	10 (6.3)	1.44 (64)	0.140 (43)
Hi[b]	25.3	2.52	0.207
Lo[b]	3.03	0.51	0.081

Values from Table 3 used to calculate all partition coefficients and exchange coefficients.
Parenthetical values represent 1σ SDOM and are always larger than the 2σ AU.
[a]Values computed using apatite-melt pairs from Tables S7–S10
[b]Values do not include results from apatite-melt pairs

This is a preprint, the final version is subject to change, of the American Mineralogist (MSA)
Cite as Authors (Year) Title. American Mineralogist, in press.
DOI: https://doi.org/10.2138/am-2018-6339

Figure Captions

Figure 1. Backscattered electron images of experimental run products from experiments a) Q1b.005, b) Q1.006, c) Q1.007, and d) Q1.012. All phases present are labeled as follows: M – melt (if more than one melt is present then a subscript L or D appears to distinguish between lighter-colored melt (M_L) and darker-colored melt (M_D) in the BSE images, respectively), Ap – apatite, Px – pyroxene, Si – silica, Ilm – ilmenite, Pl – plagioclase.

Figure 2. Melt-melt partitioning data of F and Cl between the two conjugate liquids within each of the experiments that underwent SLI. Data within this plot are from Tables S2-S6 and represent both SiO_{2Max}/SiO_{2Min} values and $SiO_2>X/SiO_2<Y$ values (defined in Tables S2-S6). Fluorine data are represented by purple circles, and Cl data are represented by green circles. The D values were obtained by dividing the concentration (wt.%) of component X in the Si-rich melt by the concentration (wt.%) of component X in the Si-poor melt. The ΔSiO_2 values were computed by subtracting the average SiO_2 abundance of the Si-poor melt composition from the average SiO_2 abundance of the Si-rich melt composition.

Figure 3. Plots of $K_{d_{Cl-F}}^{Ap-Melt}$ values versus F or Cl abundances in apatite or silicate melt. Error bars on the $K_{d_{Cl-F}}^{Ap-Melt}$ values were derived from propagating the standard deviation of the mean from each average analysis through the K_d value. a) F in apatite, b) Cl in apatite, c) F in silicate melt, and d) Cl in silicate melt. Data from McCubbin et al (2015b) are shown with orange squares, and the pink shaded region in each plot represents the average $K_{d_{Cl-F}}^{Ap-Melt}$ value of 0.21 ± 0.03 determined by McCubbin et al. (2015b). The legend in Figure 3a applies to panels a-d. *Data published by McCubbin et al. (2015b).

Figure 4. Ternary plot of F-Cl-OH components in apatite with regions shaded in white to indicate apatite compositions that are likely to have constant apatite-melt exchange K_d's (OH-F, OH-Cl, and Cl-F) adapted from McCubbin et al. (2015b). Regions of the ternary shaded in grey

indicate apatite compositions that may deviate from apatite-melt exchange K_d's (OH-F, OH-Cl, and Cl-F) determined in McCubbin et al. (2015b). Apatite compositions from each of the apatite-bearing experiments are plotted in blue (1050 °C), yellow (1000 °C), and red (950 °C). All apatites from the present study were forced to the F-Cl binary join based on their F-Cl ratio given the paucity of OH in the experiments. The orange square data points represent the apatites from McCubbin et al. (2015b). Area of shaded regions were estimated from the apatite-melt partitioning results obtained experimentally in this study, McCubbin et al. (2015b), and they were inferred from previously published thermodynamic data (excess enthalpies of mixing) for the OH-F apatite binary joins from Hovis et al. (2014). For the portion of the ternary constrained only by excess enthalpy of mixing data for binary F-OH apatite, we have used a dashed line to indicate a higher degree of uncertainty in this region. The exchange K_d values themselves can vary as a function of P and T, so the geometry of the shaded and unshaded fields in the ternary are relevant to the pressure range of 0–1.2 GPa and temperature range of 950–1050 °C. *Data published by McCubbin et al. (2015b).

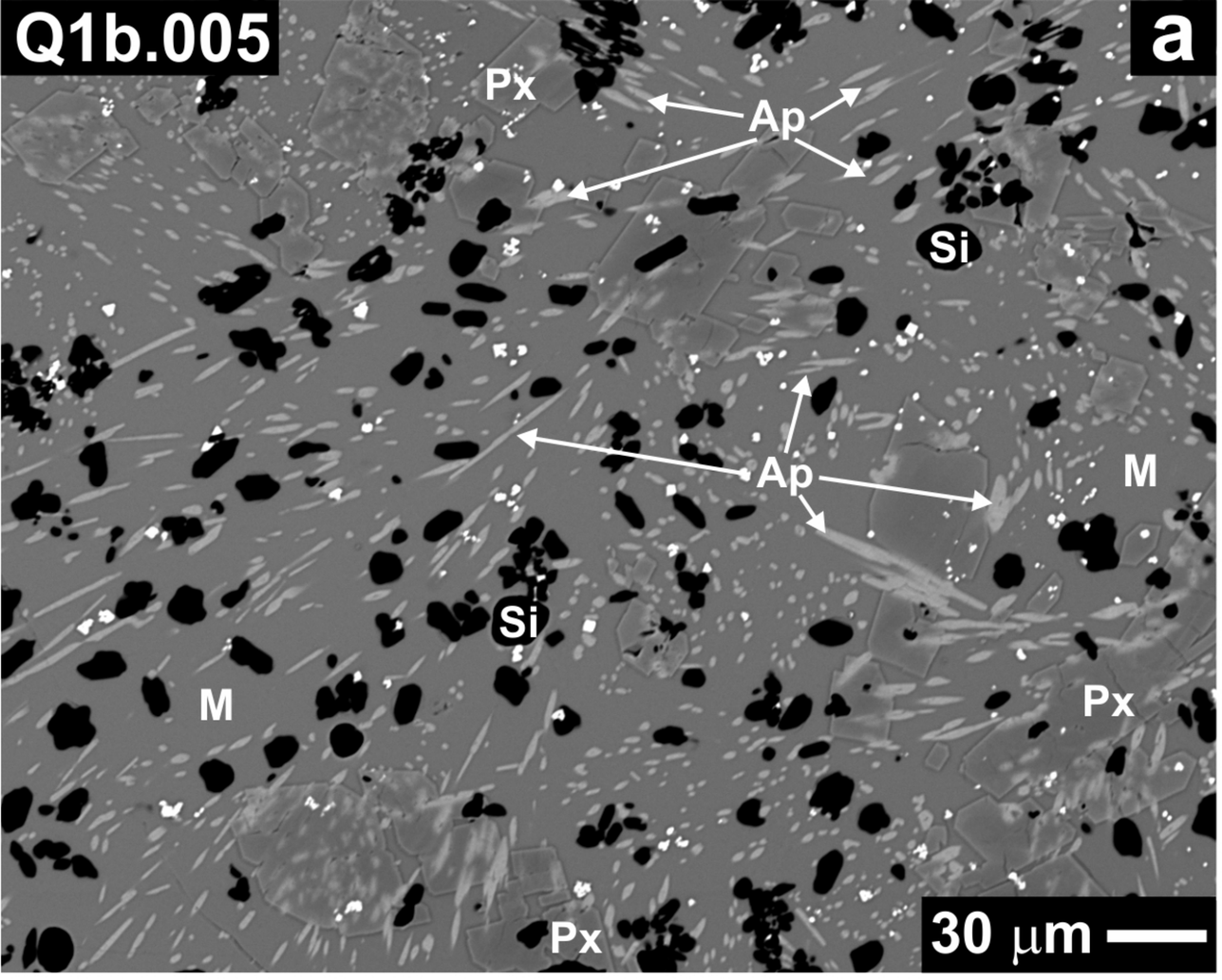
Q1b.005
a
Px
Ap
Si
Ap
M
Si
M
Px
Px
30 μm

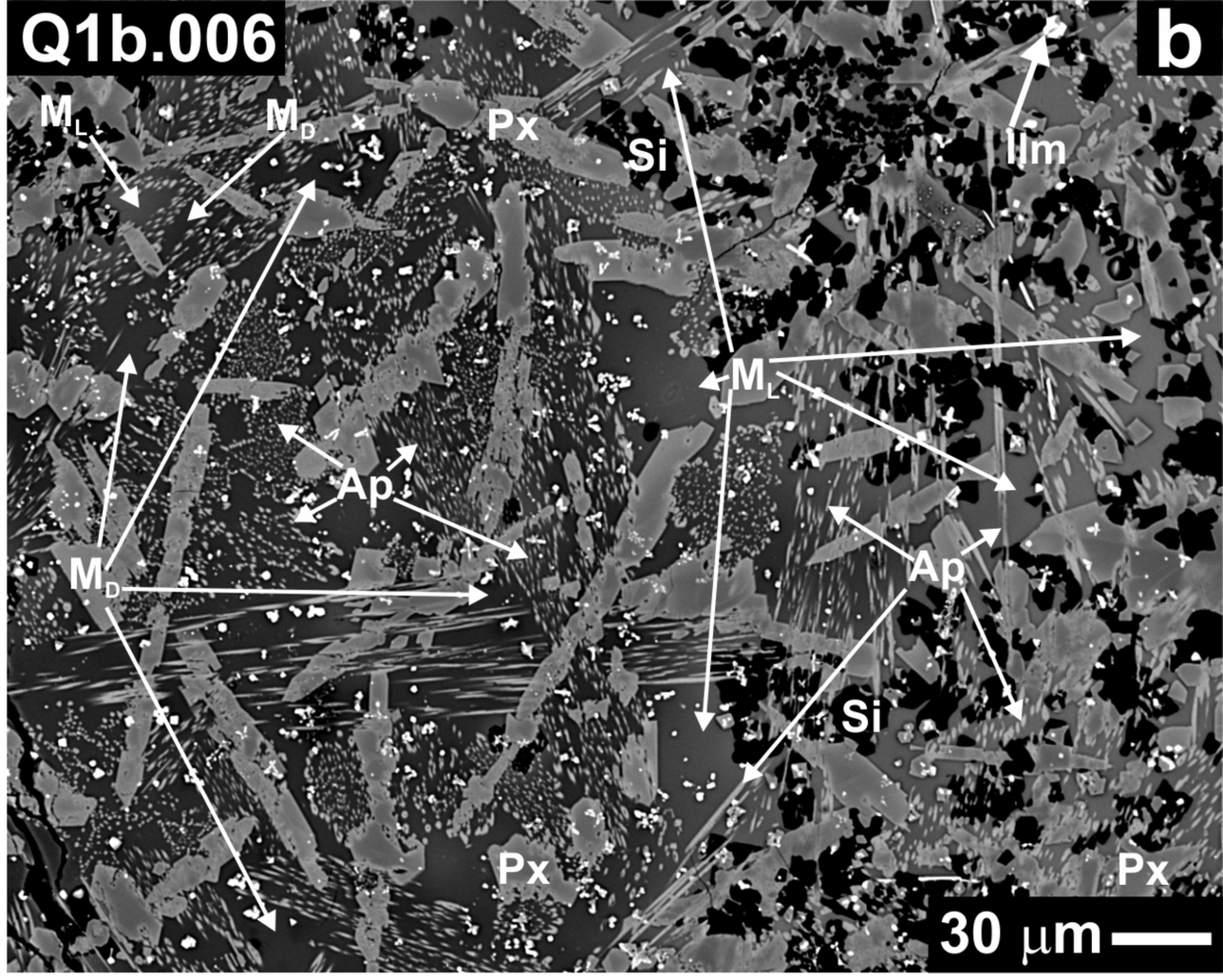
Q1b.006
b
M_L
M_D
Px
Si
Ilm
M_L
Ap
M_D
Ap
Si
Px
Px
30 μm

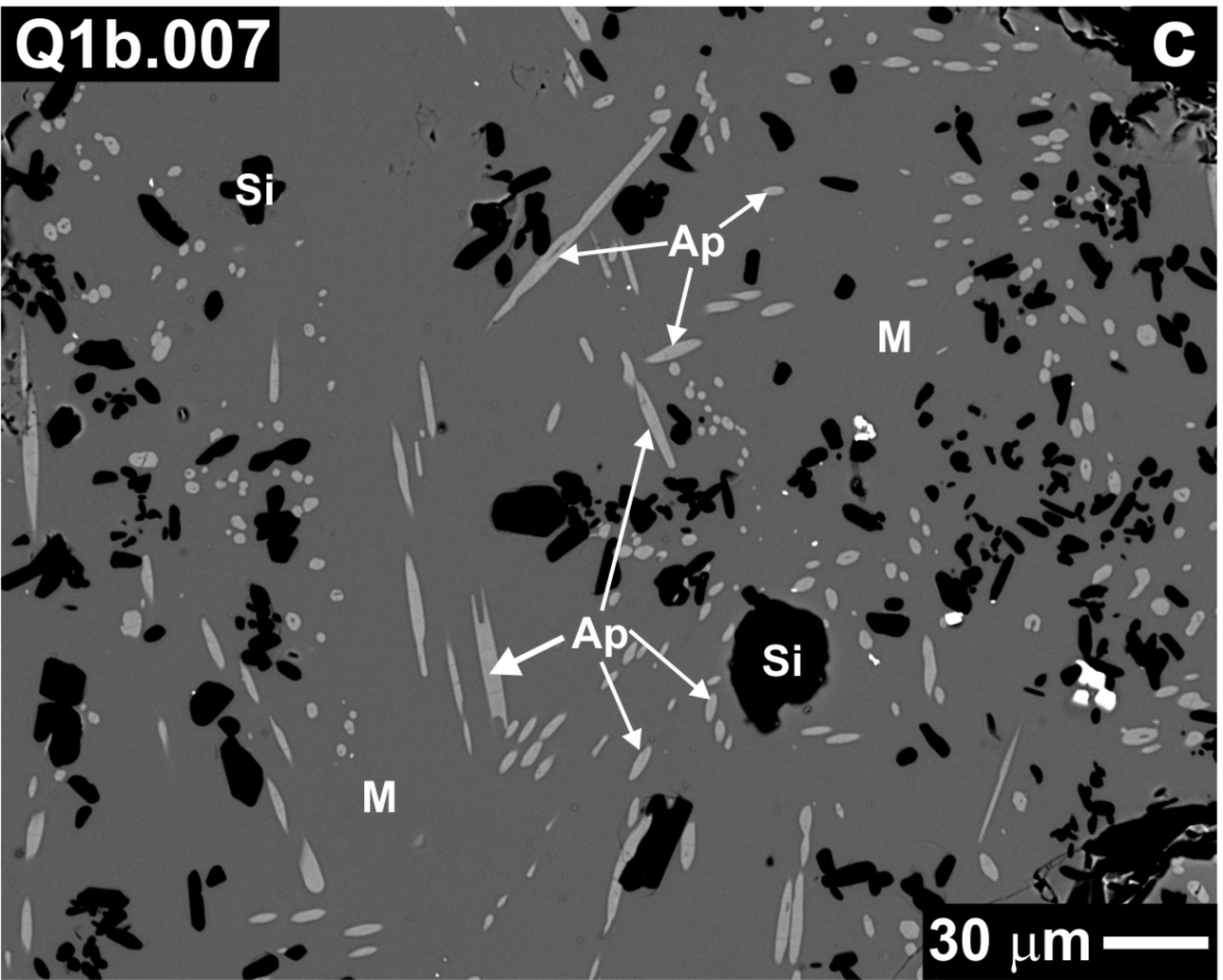
Q1b.007
c
Si
Ap
M
Ap
Si
M
30 μm

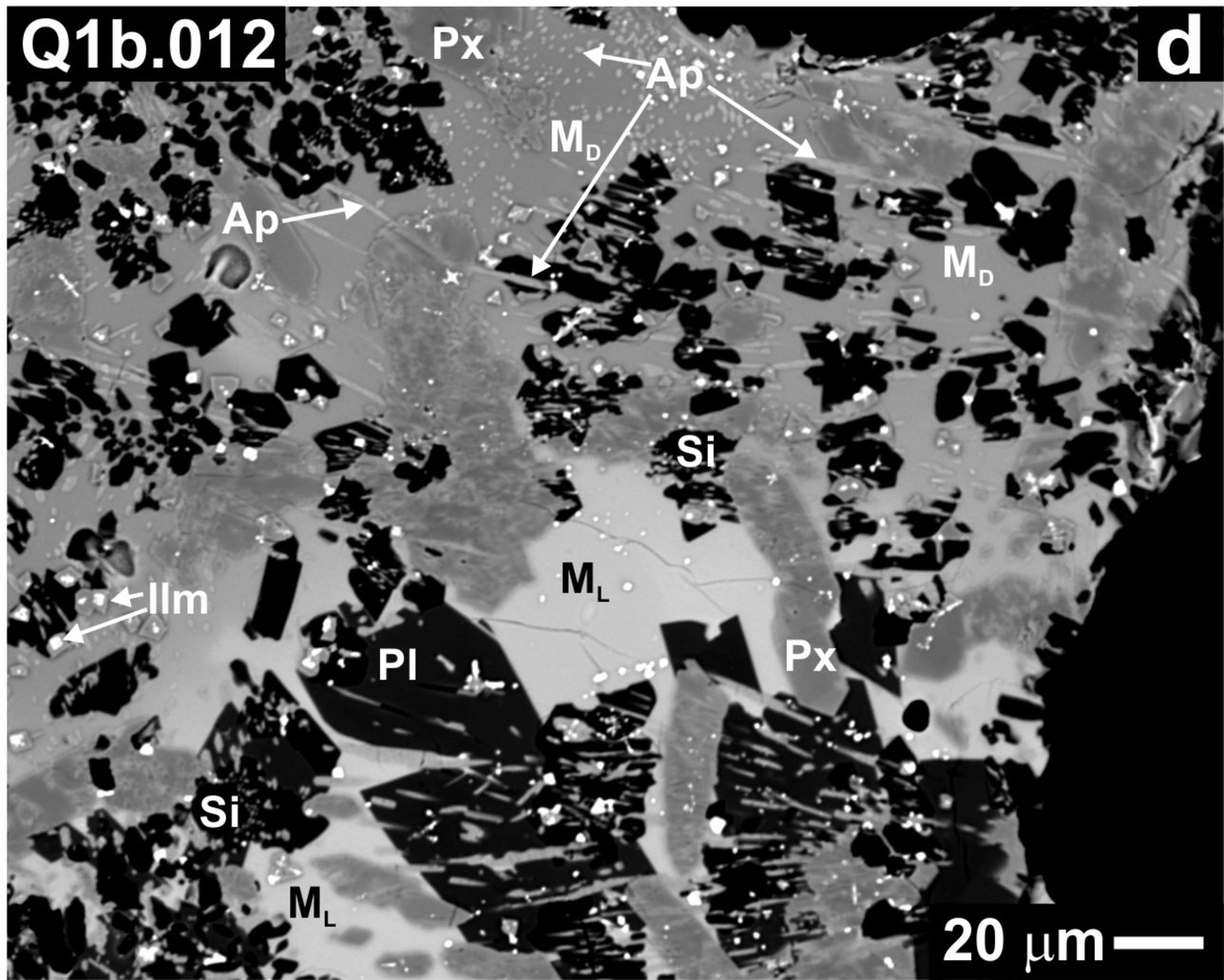
Q1b.012
d
Px
Ap
M_D
Ap
M_D
Si
Ilm
M_L
Pl
Px
Si
M_L
20 μm

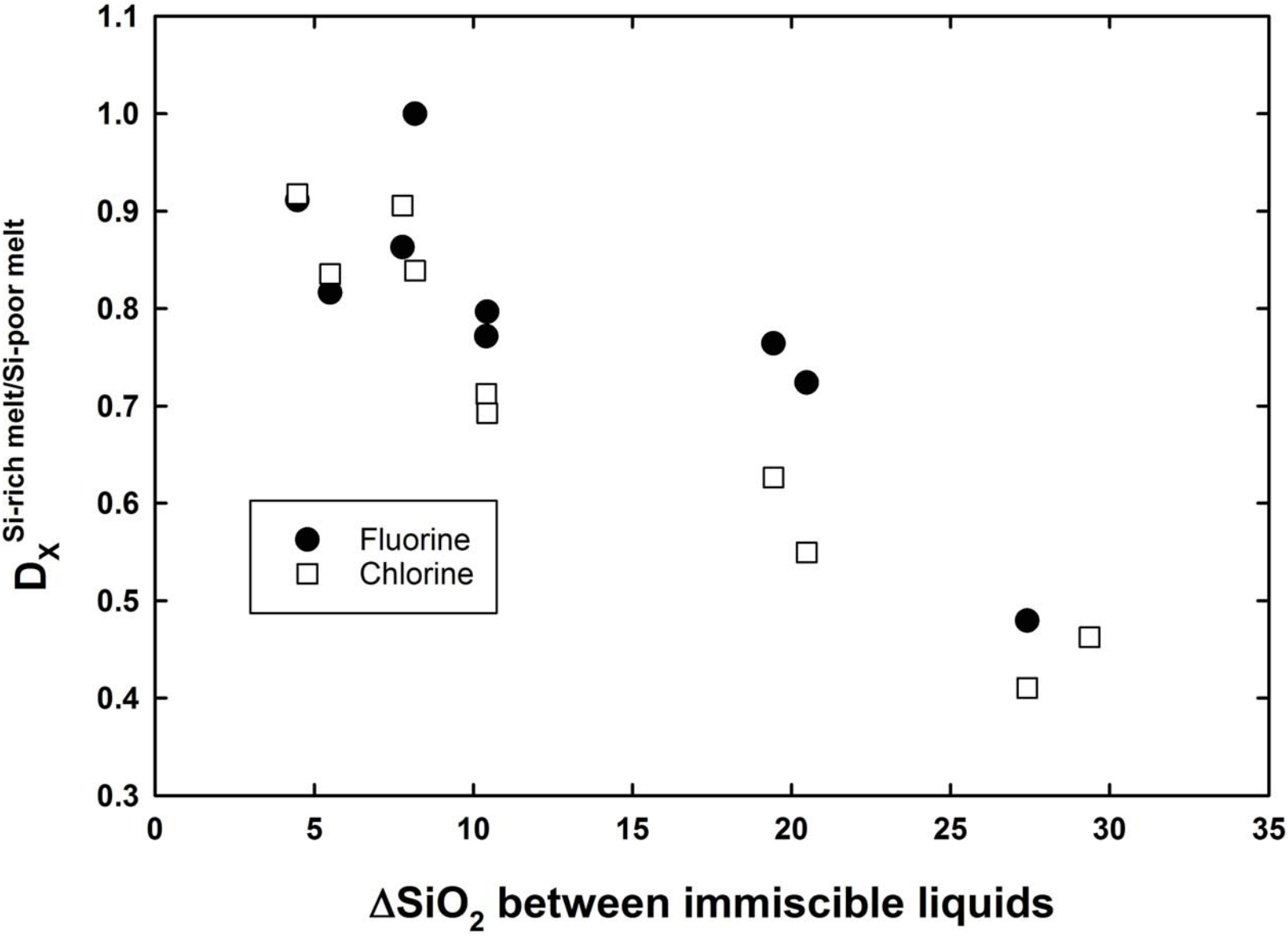
1.1
1.0
0.9
0.8
0.7
0.6
0.5
0.4
0.3
0
5
10
15
20
25
30
35
D_X Si-rich melt/Si-poor melt
Fluorine
Chlorine
ΔSiO_2 between immiscible liquids

a

0 GPa 1050 °C
0 GPa 1000 °C
0 GPa 950 °C
1-1.2 GPa 950-1000 °C*

$Kd_{Cl-F}^{Ap-Melt}$

F Apatite (sfu)

b

$Kd_{Cl-F}^{Ap-Melt}$

Cl Apatite (sfu)

c

$Kd_{Cl-F}^{Ap-Melt}$

F Melt (wt.%)

d

$Kd_{Cl-F}^{Ap-Melt}$

Cl Melt (wt.%)

Cl

- 0 GPa 1050 °C
- 0 GPa 1000 °C
- 0 GPa 950 °C
- 1-1.2 GPa 950-1000 °C*

Region of constant K_d values

Region of variable K_d values

OH

F